Cell

Chimeric contribution of human extended pluripotent stem cells to monkey embryos *ex vivo*

Graphical abstract

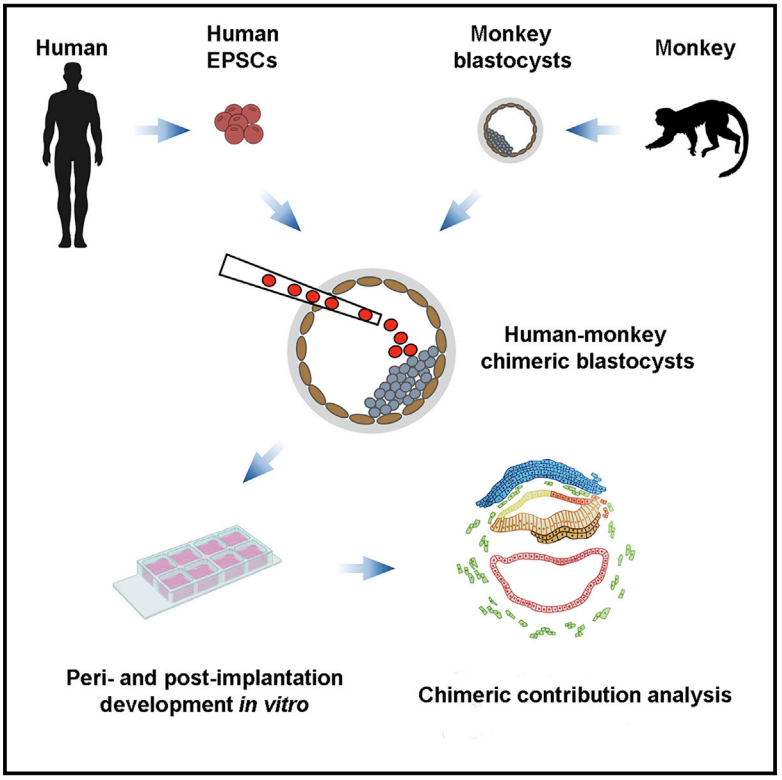

Highlights

- Generation of human-monkey chimeric embryos *ex vivo* with hEPSCs
- hEPSCs differentiated into hypoblast and epiblast lineages
- scRNA-seq analyses revealed developmental trajectories of human and monkey cells
- The approach may allow for enhancing chimerism between evolutionarily distant species

Authors

Tao Tan, Jun Wu, Chenyang Si, ..., Weizhi Ji, Yuyu Niu, Juan Carlos Izpisua Belmonte

Correspondence

tant@lpbr.cn (T.T.), jun2.wu@utsouthwestern.edu (J.W.), wji@lpbr.cn (W.J.), niuyy@lpbr.cn (Y.N.), belmonte@salk.edu (J.C.I.B.)

In brief

Human cells, in the form of extended pluripotent stem cells, have the ability to contribute to both embryonic and extra-embryonic lineages in *ex-vivo*-cultured monkey embryos.

Tan et al., 2021, Cell *184*, 2020–2032
April 15, 2021
https://doi.org/10.1016/j.cell.2021.03.020

CellPress

Cell

Article

Chimeric contribution of human extended pluripotent stem cells to monkey embryos *ex vivo*

Tao Tan,[1,4,*] Jun Wu,[2,4,5,*] Chenyang Si,[1,4] Shaoxing Dai,[1,4] Youyue Zhang,[1,4] Nianqin Sun,[1] E Zhang,[1] Honglian Shao,[1] Wei Si,[1] Pengpeng Yang,[1] Hong Wang,[1] Zhenzhen Chen,[1] Ran Zhu,[1] Yu Kang,[1] Reyna Hernandez-Benitez,[2] Llanos Martinez Martinez,[3] Estrella Nuñez Delicado,[3] W. Travis Berggren,[2] May Schwarz,[2] Zongyong Ai,[1] Tianqing Li,[1] Concepcion Rodriguez Esteban,[2] Weizhi Ji,[1,*] Yuyu Niu,[1,*] and Juan Carlos Izpisua Belmonte[2,6,*]

[1]State Key Laboratory of Primate Biomedical Research, Institute of Primate Translational Medicine, Kunming University of Science and Technology, Kunming, Yunnan 650500, China

[2]Gene Expression Laboratory, Salk Institute for Biological Studies, La Jolla, CA 92037, USA

[3]Universidad Católica San Antonio de Murcia (UCAM), Campus de los Jerónimos, No 135 12, Guadalupe 30107, Spain

[4]These authors contributed equally

[5]Present address: Department of Molecular Biology, University of Texas Southwestern Medical Center, Dallas, TX 75390, USA

[6]Lead contact

*Correspondence: tant@lpbr.cn (T.T.), jun2.wu@utsouthwestern.edu (J.W.), wji@lpbr.cn (W.J.), niuyy@lpbr.cn (Y.N.), belmonte@salk.edu (J. C.I.B.)

https://doi.org/10.1016/j.cell.2021.03.020

SUMMARY

Interspecies chimera formation with human pluripotent stem cells (hPSCs) represents a necessary alternative to evaluate hPSC pluripotency *in vivo* and might constitute a promising strategy for various regenerative medicine applications, including the generation of organs and tissues for transplantation. Studies using mouse and pig embryos suggest that hPSCs do not robustly contribute to chimera formation in species evolutionarily distant to humans. We studied the chimeric competency of human extended pluripotent stem cells (hEPSCs) in cynomolgus monkey (*Macaca fascicularis*) embryos cultured *ex vivo*. We demonstrate that hEPSCs survived, proliferated, and generated several peri- and early post-implantation cell lineages inside monkey embryos. We also uncovered signaling events underlying interspecific crosstalk that may help shape the unique developmental trajectories of human and monkey cells within chimeric embryos. These results may help to better understand early human development and primate evolution and develop strategies to improve human chimerism in evolutionarily distant species.

INTRODUCTION

Pluripotent stem cells (PSCs) are capable of indefinite self-renewal in culture and generating all adult cell types (De Los Angeles et al., 2015; Hackett and Surani, 2014; Rossant and Tam, 2017; Wu and Izpisua Belmonte, 2016). PSCs have recently been harnessed for interspecies organogenesis via blastocyst complementation, a technique that holds potential to provide large quantities of *in-vivo*-generated human cells, tissues, and organs for regenerative medicine applications, including organ transplantation (Suchy and Nakauchi, 2018; Wu et al., 2016). One of the requirements for successful interspecies blastocyst complementation with human PSCs (hPSCs) is their ability to contribute to chimera formation. The chimeric competency of hPSCs has been systematically tested in several animal species (Wu et al., 2016), but despite sustained efforts from different laboratories, the general consensus is that hPSCs do not consistently and robustly contribute to chimera formation when the host animal has a high evolutionary distance from humans (e.g., mice and pigs; Wu et al., 2016, 2017). This is the case even when human cell apoptosis is inhibited (Das et al., 2020; Huang et al., 2018; Wang et al., 2018). Xenogeneic barriers between hPSCs and evolutionarily distant host animal species have been suggested to account for limited chimerism (Wu et al., 2016, 2017), though the use of hPSCs for chimera studies in host species evolutionarily close to humans remains unexplored to date.

Cultured PSCs reflect the continuum of pluripotency that is seen *in vivo*, and different cell culture formulations result in distinct pluripotency states *in vitro* (Morgani et al., 2017; Smith, 2017; Weinberger et al., 2016). hPSCs in different pluripotency states exhibit distinct transcriptional, epigenetic, and metabolic features. They also differ in their chimeric potential when introduced into animal embryos (De Los Angeles, 2019; Harvey et al., 2019; Zhang et al., 2018). Recently, we and others identified human extended PSCs (hEPSCs) that demonstrated improved chimeric capability in mouse conceptuses (Gao et al., 2019; Yang et al., 2017b). To date, however, the chimeric competency of hEPSCs has not been determined in other species.

Leveraging a recently developed culture system that enables cynomolgus monkey (monkey for short) embryos to develop up to 20 days *ex vivo* (Ma et al., 2019; Niu et al., 2019), we performed microinjection of hEPSCs into monkey blastocysts and examined their contribution to cultured monkey embryos at different time points (Figure 1A). We found that hEPSCs could integrate into the inner cell masses (ICMs) of late monkey blastocysts and contributed to both embryonic and extra-embryonic lineages in peri- and early post-implantation stages during prolonged embryo culture. We also determined the differentiation trajectory of hEPSCs within cultured monkey embryos by single-cell RNA sequencing (scRNA-seq) analysis.

RESULTS

Generation of human-monkey chimeric blastocysts *in vitro*

To determine the chimera competency of hPSCs in a closely related non-human primate species, we used a well-characterized hEPSC line generated by cellular reprogramming, iPS1-EPSCs, which demonstrated improved chimerism in embryonic day 10.5 (E10.5) mouse conceptuses over other reported hPSCs (Yang et al., 2017b). Consistent with the previous report, iPS1-EPSCs exhibited a dome-shaped colony morphology and expressed the core pluripotency transcription factors OCT4, NANOG, and SOX2 (Figure S1A). To generate human-monkey chimeric embryos, early blastocysts from cynomolgus monkeys (6 days post-fertilization [d.p.f.6]) were injected with 25 iPS1-EPSCs labeled with tdTomato (TD). Injected embryos were first cultured to the late blastocyst stage (d.p.f.7) for analysis. The proliferation of hEPSCs within monkey blastocysts was evident (Video S1). In total, TD^+ iPS1-EPSCs were detected in all d.p.f.7 monkey blastocysts (100%, n = 132) (Figure S1B).

Chimeric contribution of hEPSCs to peri- and post-implantation monkey embryos

We next took advantage of a recently established prolonged embryo culture system that supports *ex vivo* primate (human and monkey) embryogenesis to the gastrulation stage (Deglincerti et al., 2016; Ma et al., 2019; Niu et al., 2019; Shahbazi et al., 2016; Xiang et al., 2020; Zhou et al., 2019). In this embryo culture system, the zona pellucida is removed and the denuded blastocysts are allowed to attach to the culture dish for further development. We used this system to trace the fate of hEPSCs in monkey embryos at peri- and post-implantation stages. Similar to noninjected controls (92.31%, n = 104) (Niu et al., 2019), most embryos injected with hEPSCs attached at approximately d.p.f.10 (92.79%, n = 111). After attachment, the injected embryos continued to grow, and an embryonic disc became visible at approximately d.p.f.11 as seen with controls (Figure 1B). TD^+ human cells were found in the embryonic disc of more than half of the injected embryos at d.p.f. 9, but this ratio progressively declined at approximately one-third by d.p.f.13 (Figure 1C). To determine whether introduced hEPSCs may affect embryo development, we evaluated and compared the developmental status of injected and control embryos (Niu et al., 2019). We found that the developmental ratios of injected embryos were slightly lower than that of controls (Figure 1D). Furthermore, similar to controls, the developmental ratios of injected embryos dropped sharply at approximately d.p.f.15, which may reflect the limitation of the 2D attachment embryo culture system (Figure 1D).

To study the developmental potential of hEPSCs in monkey embryos, we performed immunofluorescence (IF) studies using antibodies specific for several embryonic and extra-embryonic lineages. Analyses were performed between d.p.f.9 and d.p.f.19. At the peri-implantation stage (d.p.f.9), on average, 10.2 ± 7.2 (n = 9) iPS1-EPSCs were found incorporated into the ICM (the number of TD^+OCT4^+ cells found within or close to $NANOG^+$ or $OCT4^+$ monkey cells) (Figure 2A). Although these cells expressed OCT4, only a few of them expressed NANOG (Figure S1C). Supporting their epiblast (EPI)-like identity, we did not observe GATA6 (a hypoblast [HYP] marker) expression in these cells (Figure S1C). In addition, TD^+GATA4^+ HYP-like cells were also detected (Figure 2B). In contrast to the results reported in mice (Yang et al., 2017b), only a few iPS1-EPSCs were detected in the trophectoderm (TE) layer of monkey blastocysts and expressed TE (TE or trophoblast) marker genes (e.g., TFAP2C and CK7) (Figure 2C).

At d.p.f.11, TD^+OCT4^+cells were also detected in the EPI layer of monkey embryos, and these cells rarely expressed T^+ (also known as Brachyury), a marker of gastrulation. By contrast, T^+ monkey cells were detected at the dorsal amnion of the embryos (Figure 2D). In addition, TD^+ human cells expressing a HYP marker, platelet-derived growth factor receptor-alpha (PDGFRα), were found intermingled within monkey HYP cells (Figure 2E). $OCT4^+$ human cells expressing COL6A1, a marker of extra-embryonic mesenchyme cells (EXMCs), were found outside of the EPI layer, suggesting ongoing differentiation of hEPSCs toward EXMCs (Figure S1D). At d.p.f.13, hEPSCs were detected beneath the EPI layer and expressed an endoderm marker, SOX17, suggesting that they have initiated gastrulation (Figure 2F). Interestingly, we found that from d.p.f.13 onward human cells tended to group together and segregate from the monkey EPI layer. These human cells appeared to undergo differentiation into gastrulating cells as evidenced by the gained expression of OTX2 (Martyn et al., 2018; Vincent et al., 2003) while maintaining OCT4 expression (Figure S1E). Overall, we found that hEPSCs exhibited reasonable contribution to the EPI (with the highest contribution of 7.08% observed at d.p.f.15), relatively lower contribution to the HYP (with the highest contribution of 4.96% observed at d.p.f.19), and limited contribution to the TE in peri- and post-implantation monkey embryos (Figure 2G).

Transcriptional landscape of human-monkey chimeric embryos

To further delineate the developmental trajectory of human-monkey chimeric embryos, scRNA-seq analysis was carried out to profile the transcriptomes of human and monkey cells at different developmental stages. Following embryo dissociation, single human (TD^+) and monkey (TD^-) cells were manually collected using fluorescence microscopy and subjected to scRNA-seq. In total, we sequenced 227 human and 302 monkey cells isolated from chimeric embryos at different time points during *ex vivo* culture (d.p.f.9–d.p.f.17; Table S2). TD expression and

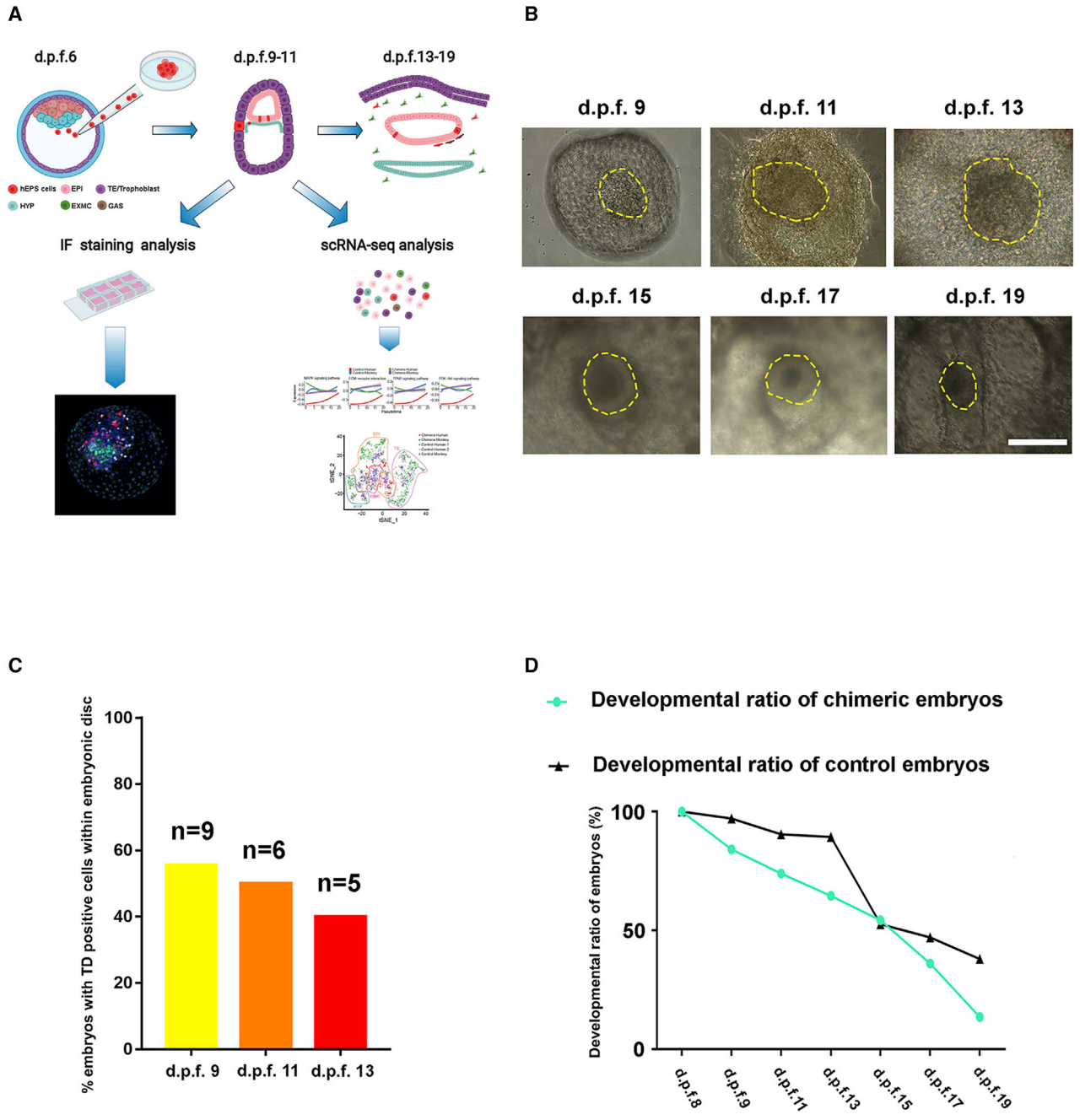

Figure 1. Generation and developmental capability of human-monkey *ex-vivo* chimeras

(A) Schematic of the generation and analyses of chimeric embryos derived from blastocyst injection of hEPSCs (created with BioRender.com). hEPSCs, human extended pluripotent stem cells; EPI, epiblast; HYP, hypoblast; TE, trophectoderm; EXMC, extra-embryonic mesenchyme cell; GAS, gastrulating cell; IF, immunofluorescence.

(B) Representative bright-field images of hEPSC-injected monkey embryos cultured *in vitro* until d.p.f.19 (n = 111 embryos for d.p.f.9; n = 91 embryos for d.p.f.11; n = 60 embryos for d.p.f.13; n = 38 embryos for d.p.f.15; n = 12 embryos for d.p.f.17 and n = 3 embryos for d.p.f.19). Scale bar, 100 μm. Yellow dotted lines indicate ICM (d.p.f.9) or embryonic disc (d.p.f.11 to d.p.f.19).

(C) Histogram showing the percentages of host monkey embryos containing human cells within ICM or embryonic disc (yellow dotted lines in B).

(D) Dynamics of developmental ratios of chimeric (n = 126, d.p.f.8) and non-chimeric monkey embryos (n = 104, data from Niu et al., 2019). Embryos without clear embryonic disc structure and/or appear dead were excluded from the analysis.

See also Figure S1 and Video S1.

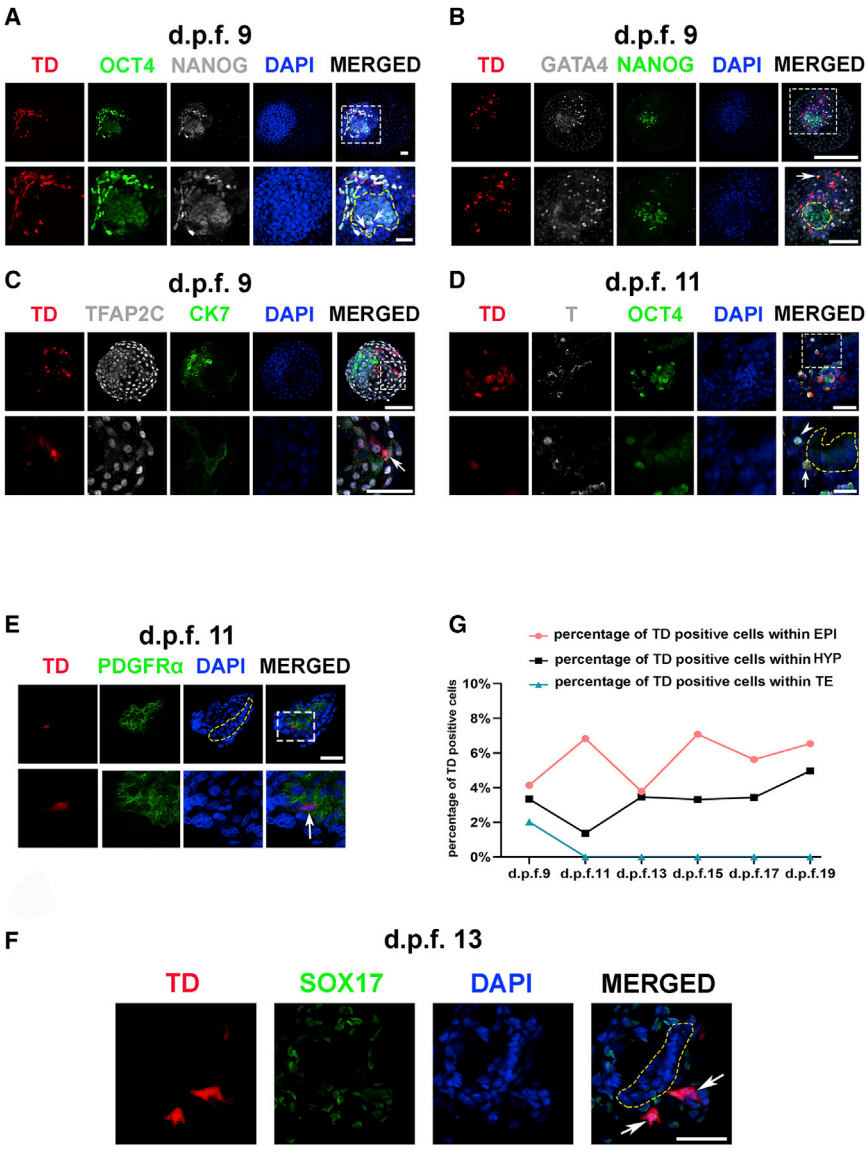

Figure 2. hEPSCs contribute to chimera formation in peri- and post-implantation monkey embryos

(A) Representative IF images showing integration of TD-positive hEPSCs into ICM of host monkey embryos at d.p.f.9 (n = 7). The embryos were stained for OCT4 (green) and NANOG (gray). Scale bar, 250 μm. Bottom, enlargements of the insert (white dotted line) in the top panel. Arrows indicate TD-positive hEPSCs expressing OCT4 and NANOG. Yellow dotted line indicates ICM. Scale bar, 50 μm.

(B) Representative IF images showing hEPSCs differentiated into HYP-like cells within host monkey embryos at d.p.f.9. The embryos were stained for GATA4 (gray) and NANOG (green). Scale bar, 250 μm. Bottom, enlargements of the insert (white dotted line) in the top panel. Arrow indicates a TD-positive hEPSC expressing GATA4. Yellow dotted line indicates ICM. Scale bar, 100 μm.

(C) Representative IF images showing integration of TD-positive hEPSCs into TE of host monkey embryos at d.p.f.9 (n = 3). The embryos were stained for TFAP2C (gray) and CK7 (green). Scale bar, 100 μm. Bottom, enlargements of the insert (white dotted line) in the top panel. Arrow indicates a TD-positive hEPSC expressing TFAP2C and CK7. Scale bar, 50 μm.

(D) Representative IF images showing incorporation of hEPSCs into EPI of host monkey embryo at d.p.f.11 (n = 3). The embryos were stained for T (gray) and OCT4 (green). Scale bar, 250 μm. Bottom: enlargements of inserts (white dotted line) in the top panel. Notably, hEPSCs rarely express T (arrow), a marker of mesoderm, whereas the expression of T is detected in monkey cells (arrowhead). Yellow dotted line indicates EPI. Scale bar, 25 μm.

(E) Expression of HYP marker, PDGFRα, in hEPSCs at d.p.f.11 (n = 2). The embryos were stained for PDGFRα (green). Scale bar, 50 μm. Bottom: enlargements of the insert (white dotted line) in the top panel. Arrow indicates a tdTomato-positive hEPSC expressing PDGFRα. Yellow dotted line indicates EPI. Scale bar, 10 μm.

(F) IF images of sections of monkey embryos at d.p.f.13 (n = 5) staining for SOX17 (green). Arrows indicate tdTomato-positive hEPSCs expressing SOX17. Scale bar, 50 μm. Yellow dotted line indicates EPI.

(G) Levels of chimerism of hEPSCs within EPI, HYP, and TE. EPI cells expressed only OCT4, and HYP cells expressed GATA6 and/or GATA4, whereas TE expressed CK7 (a total of 25 embryos and 17,938 cells were analyzed). EPI, epiblast; HYP, hypoblast; TE, trophectoderm; TD, tdTomato; DAPI, 4′,6-diamidino-2-phenylindole. See also Figure S1.

the ratio of reads mapped to the human or cynomolgus monkey genomes were used to further confirm each cell's species of origin (Figures S2A and S2B). After stringent filtering, 200 human and 272 monkey cells were used for further analyses (Table S2). On average, 9,798 genes (transcripts per million [TPM] > 0) and 27,936,953 reads were detected per cell. There was no statistical difference in the number of genes and reads detected between human and monkey cells (Figure S2C). For comparison, we also included published scRNA-seq datasets containing cells from monkey and human embryos in the analyses (Nakamura et al., 2016; Niu et al., 2019; Xiang et al., 2020; Zhou et al., 2019). To avoid batch-specific systematic variations of scRNA-seq caused by integration of different datasets, we used an "anchors" method that is recommended for batch-effect removal (Stuart et al., 2019) (Figure S2C).

We first performed t-distributed stochastic neighbor embedding (t-SNE) analysis on the scRNA-seq datasets. Based on the expression of known lineage markers, we identified four major cell clusters that were present in all samples (both chimeric and control embryos): EPI, HYP, TE, and EXMC (Figures 3A, 3B, and S2D). These cells also expressed lineage-specific markers that showed conservation between humans and

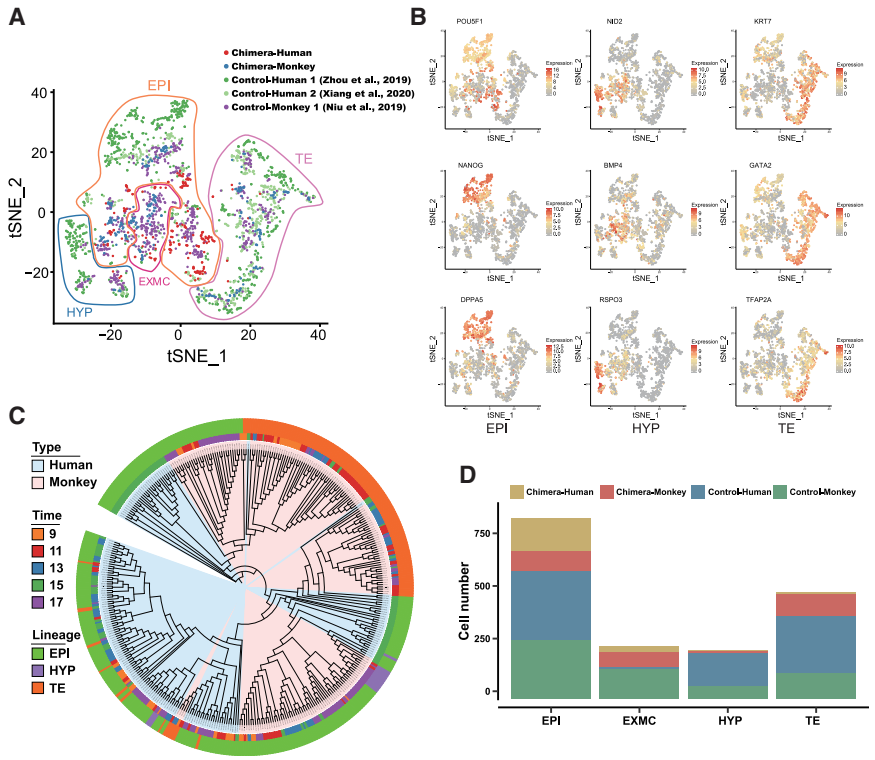

Figure 3. Transcriptional landscape of human-monkey chimeric embryos

(A) t-SNE plot of cells from chimeric and control non-chimeric embryos. Cells were identified as EPI, HYP, TE, and EXMC. Cells were colored by different species origins and datasets.

(B) Expression of lineage-specific marker genes of EPI, HYP, and TE exhibited on t-SNE plots. A gradient of gray, yellow, and red indicates low to high expression.

(C) The phylogenetic tree shows the cluster of EPI, HYP, and TE cells from chimeric embryos at different stages (d.p.f.9, 11, 13, 15, and 17). Cells are highlighted by species origins (human or monkey), different stages (d.p.f.9, 11, 13, 15, and 17), and different cell types (EPI, HYP, and TE).

(D) Bar plot showing the distribution of cells from different origins in the four lineages (EPI, EXMC, HYP, and TE). EPI, epiblast; HYP, hypoblast; TE, trophectoderm; EXMC, extra-embryonic mesenchyme cell.

See also Figure S2 and Table S2.

monkeys identified in a previous study (Figure S2E) (Zhou et al., 2019). The presence of these cell types in chimeric embryos suggests that the development of host embryos was by and large unaffected by the injected hEPSCs (Ma et al., 2019; Niu et al., 2019), which is consistent with the morphological analysis (Figures 1B and 1D). Interestingly, phylogenetic tree analysis (based on gene expression levels) revealed that while most monkey cells within chimeric embryos (chimeric monkey cells for short) segregated into distinct cell-type-specific clusters (EPI, HYP, and TE), chimeric human HYP- and TE-like cells clustered with EPI-like cells (Figure 3C). Thus, it seems that the chimeric monkey cells exhibited a more faithful lineage segregation than the introduced hEPSCs. In agreement with IF results, very few human TE-like cells were identified in the scRNA-seq data (Figures 3A and 3D) and were therefore excluded from subsequent analyses. Together, these results demonstrate that hEPSCs can differentiate into several peri- and early post-implantation cell types after being introduced into monkey early blastocysts followed by *ex vivo* embryo culture.

Transcriptome dynamics of hEPSCs during human-monkey chimera development

We next investigated the transcriptional kinetics of chimeric human and monkey cells. We first constructed a force-directed K-nearest neighbor graph (SPRING) (Weinreb et al., 2018) based on transcriptomic properties of all cells (see STAR Methods). All cells bifurcated into three branches: EPI, HYP, and TE (Figure 4A). The correlations of gene expression patterns between chimeric and control (human and monkey) embryos were determined (Figure 4B). Similar correlation coefficients were obtained when chimeric human cells were compared to control human (0.460) or monkey (0.459) cells (Figure 4B, right panels). Intriguingly, when compared to control embryos, chimeric monkey cells exhibited higher correlation coefficients than chimeric human cells (Figure 4B, left panels). We next generated lineage-specific correlation matrices. We found that chimeric human EPI-like cells were similar to EPI cells in human embryos, whereas chimeric human HYP- and EXMC-like cells shared the highest correlation coefficients with chimeric monkey HYP cells and EXMCs, respectively (Figure 4C). Of note, we also found that chimeric monkey EPI cells and EXMCs more resembled chimeric than control human cells. Interestingly, chimeric human EPI-like cells were found to gradually gravitate toward the chimeric monkey EPI cells, with R^2 values increasing from 0.363 (pre-implantation EPI [Pre_EPI]) to 0.464 (post-implantation late EPI [PostL_EPI]) and then to 0.693 (gastrulating [Gast] cells) (Figure 4C). Taken together, these results demonstrate that the monkey embryonic microenvironment exerts influence on the transcriptional states of human cells and vice versa.

As monkey cells exhibited transcriptomic changes in the presence of human cells, we next sought to delineate the developmental dynamics of monkey cells within chimeric embryos. We first identified differentially expressed genes (DEGs) between chimeric and control monkey embryos. Comparisons of EPI cells, HYP cells, and EXMCs revealed that 424, 7, and 241 genes were downregulated, whereas 5, 2, and 13 genes were upregulated, respectively, in cells from chimeric compared to control embryos, although the expression levels of lineage marker genes remained comparable (Figures 4D and S3A). Gene Ontology (GO) and Kyoto Encyclopedia of Genes and Genomes (KEGG) enrichment analyses identified a number of signaling pathways that were up- and downregulated in chimeric monkey EPI cells,

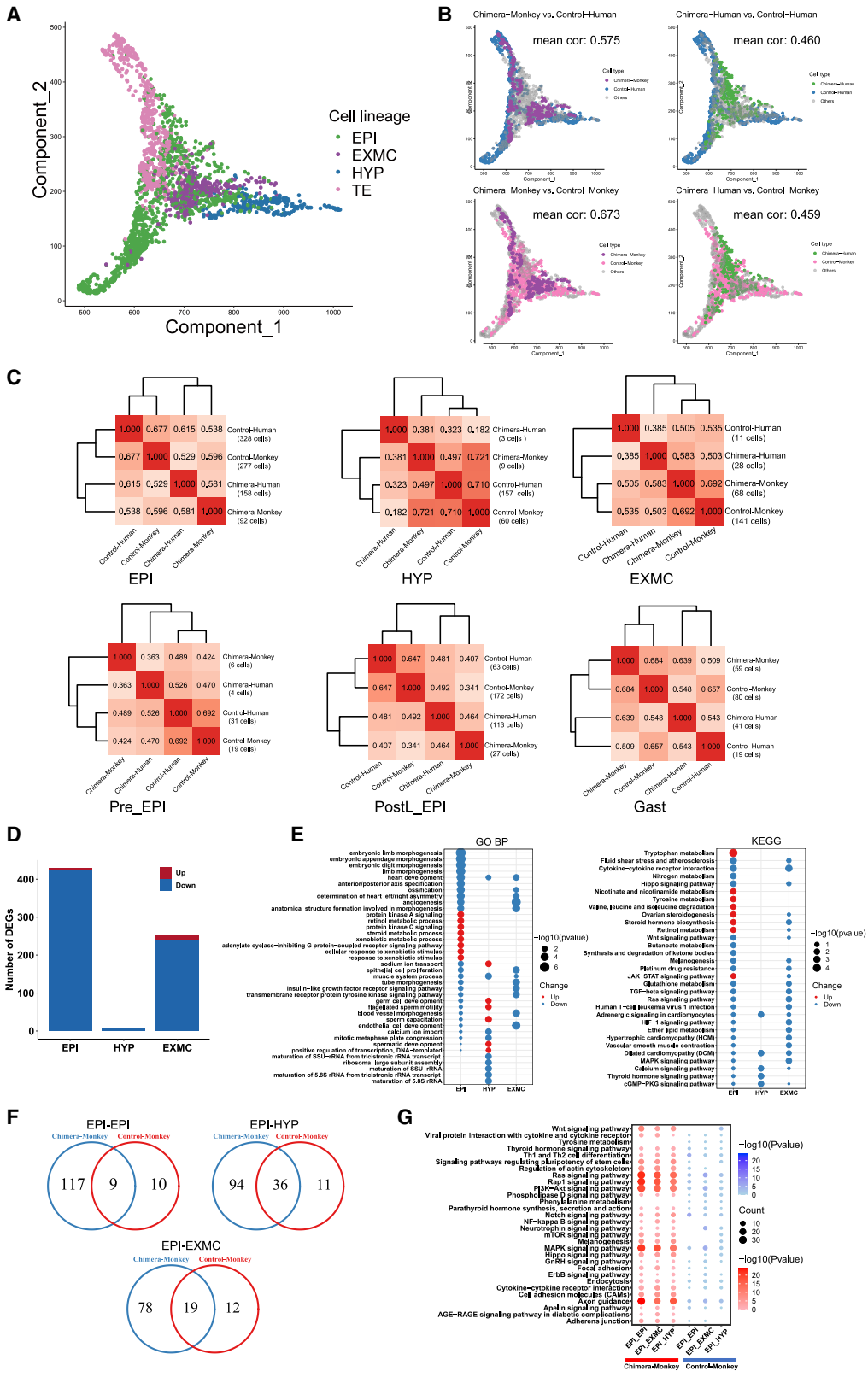

(legend on next page)

HYP cells, and EXMCs. For example, the Hippo and transforming growth factor β (TGF-β) signaling pathways were downregulated in chimeric monkey EPI cells and EXMCs (Figure 4E), respectively.

Having shown that the transcriptomic profiles of monkey EPI cells were altered in chimeric embryos, we next investigated whether the monkey EPI embryonic niche was also affected by human cells. To this end, CellPhoneDB (v2.0.1) (Vento-Tormo et al., 2018) was applied to identify potential cellular interactions between EPI and other lineages (HYP and EXMC) in both chimeric and control embryos (see STAR Methods). We sought to identify interactions that were specific to chimeric or control embryos. We found more ligand-receptor interactions in chimeric embryos when compared to control embryos (e.g., 117 [chimeric] versus 10 [control] specific ligand-receptor interactions were detected in monkey EPI cells) (Figures 4F and S3B; Table S3). KEGG analysis was performed to reveal specific signaling pathways that were enriched within chimeric and control embryos. We found several signaling pathways (e.g., phosphatidylinositol 3-kinase [PI3K]-Akt and mitogen-activated protein kinase [MAPK] signaling pathways) that were strengthened in chimeric embryos and new signaling pathways (e.g., WNT signaling pathway) that were specifically enriched in chimeric embryos (Figure 4G). Using the same method, we also determined human and monkey cell-cell interactions within chimeric embryos and identified distinct ligand-receptor interactions in EPI cells, such as FGF5-FGFR4, NOTCH4-JAG2, WNT2B-FZD4, WISP3-SORL1, and PLXNB2-PTN (Figures S3C and S3D; Table S3). Taken together, our results suggest that cell-cell interactions are reinforced within the chimeric embryos and potentially lead to activation of additional signaling pathways.

Chimeric human EPI-like cells display a distinct developmental trajectory

EPI development is characterized by pluripotency transitions that may exhibit different dynamics between species. As proper EPI specification and differentiation are critical for chimera formation and development, we examined the lineage allocation of human EPI-like cells within the chimeric embryos and compared it with the datasets of *in-vitro*-cultured human and monkey embryos (Nakamura et al., 2016; Niu et al., 2019; Zhou et al., 2019). Human EPI-like cells were identified at pre-implantation, post-implantation, and gastrulating stages, and at each stage, they expressed distinct markers (Figures 5A and S4A–S4C). A Sankey diagram also showed the same developmental dynamics of human EPI-like cells (Figure S4D). We next determined the relationship between hEPSCs (Yang et al., 2017b), chimeric human EPI-like cells, EPI cells from control human and monkey embryos (Niu et al., 2019; Zhou et al., 2019), and human and monkey PSCs (primed and naive) (Chan et al., 2013; Chen et al., 2015; Gafni et al., 2013; Theunissen et al., 2014). We observed that hEPSCs were more similar to early post-implantation EPI (PostE_EPI) and PostL_EPI cells from human and monkey embryos, respectively, as well as human and monkey naive PSCs. Chimeric human PostL_EPI-like cells showed higher correlation coefficients to primed PSCs than naive PSCs (Figure S4E). To further investigate the transcriptional kinetics of hEPSCs (Yang et al., 2017b), chimeric human EPI-like cells, and host monkey EPI cells, we performed RNA velocity (La Manno et al., 2018) and Slingshot analyses (Street et al., 2018) (Figure 5B). We observed two distinct patterns of RNA velocity vectors; chimeric human PostL_EPI-like cells bore long vectors, and gastrulating-like cells bore short vectors. In contrast, host monkey PostL_EPI cells lacked long vectors, and gastrulating cells bore long vectors (Figure 5B, left two panels). These results imply that development is delayed for chimeric human EPI-like cells. Slingshot analysis revealed that after injection into monkey blastocysts, hEPSCs followed the EPSC to PostL_EPI to gastrulation developmental trajectory (Figure 5B, right panel). To further delineate the developmental trajectory of chimeric human EPI-like cells, we mapped all EPI-related human and monkey reads to a consensus genome and aligned EPI development trajectories between species using a previously reported method (Kanton et al., 2019). In agreement with the RNA velocity analysis, we found that chimeric human EPI-like cells differentiated more slowly than EPI cells from host monkey, control monkey, and human embryos (Figure 5C). These results suggest that the specification and/or differentiation of hEPSCs toward the EPI lineages was less efficient than embryonic cells.

As mentioned above, global transcriptional profiles of chimeric human EPI-like cells more resembled monkey EPI cells within the

Figure 4. Developmental trajectory of human-monkey chimeric embryos

(A) The differentiation trajectory of chimeric cells and control non-chimeric cells. The differentiation trajectory was reconstructed using SPRING. Cells were colored by cell lineages.

(B) Overall similarity under the four comparisons (chimera-monkey versus control non-chimeric human ["Chimera-Monkey vs. Control-Human"], chimera-human versus control non-chimeric human ["Chimera-Human vs. Control-Human"], chimera-monkey versus control non-chimeric monkey ["Chimera-Monkey vs. Control-Monkey"], and chimera-human versus control non-chimeric monkey ["Chimera-Human vs. Control-Monkey"]). Cells are colored by cell origins.

(C) Heatmap of the correlation coefficients among different cell origins under corresponding lineages (EPI, EXMC, HYP, Pre_EPI, PostL_EPI, and Gast).

(D) Histogram showing the numbers of DEGs for different lineages (EPI, HYP, and EXMC) in the host monkey cells compared to cells from control non-chimeric embryos. The red and blue colors represent up- and down-regulated genes, respectively.

(E) GO and KEGG enrichment analyses of the DEGs in (D). Red and blue represent enrichment p values (−log10 transformed) for up- and downregulated DEGs, respectively.

(F) The Venn diagrams showing the overlap of the ligand-receptor interactions between EPI-EPI, EPI-HYP, and EPI-EXMC in host (Chimera-Monkey) and control non-chimeric (Control-Monkey) monkey cells.

(G) Comparison of KEGG pathways enriched by the specific interactions between host (Chimera-Monkey) and control non-chimeric (Control-Monkey) monkey cells in (F). EPI, epiblast; EXMC, extra-embryonic mesenchyme cell; HYP, hypoblast; Pre_EPI, pre-implantation EPI; PostL_EPI, post-implantation late EPI; Gast, gastrulating cell; DEG, differentially expressed gene.

See also Figure S3 and Table S3.

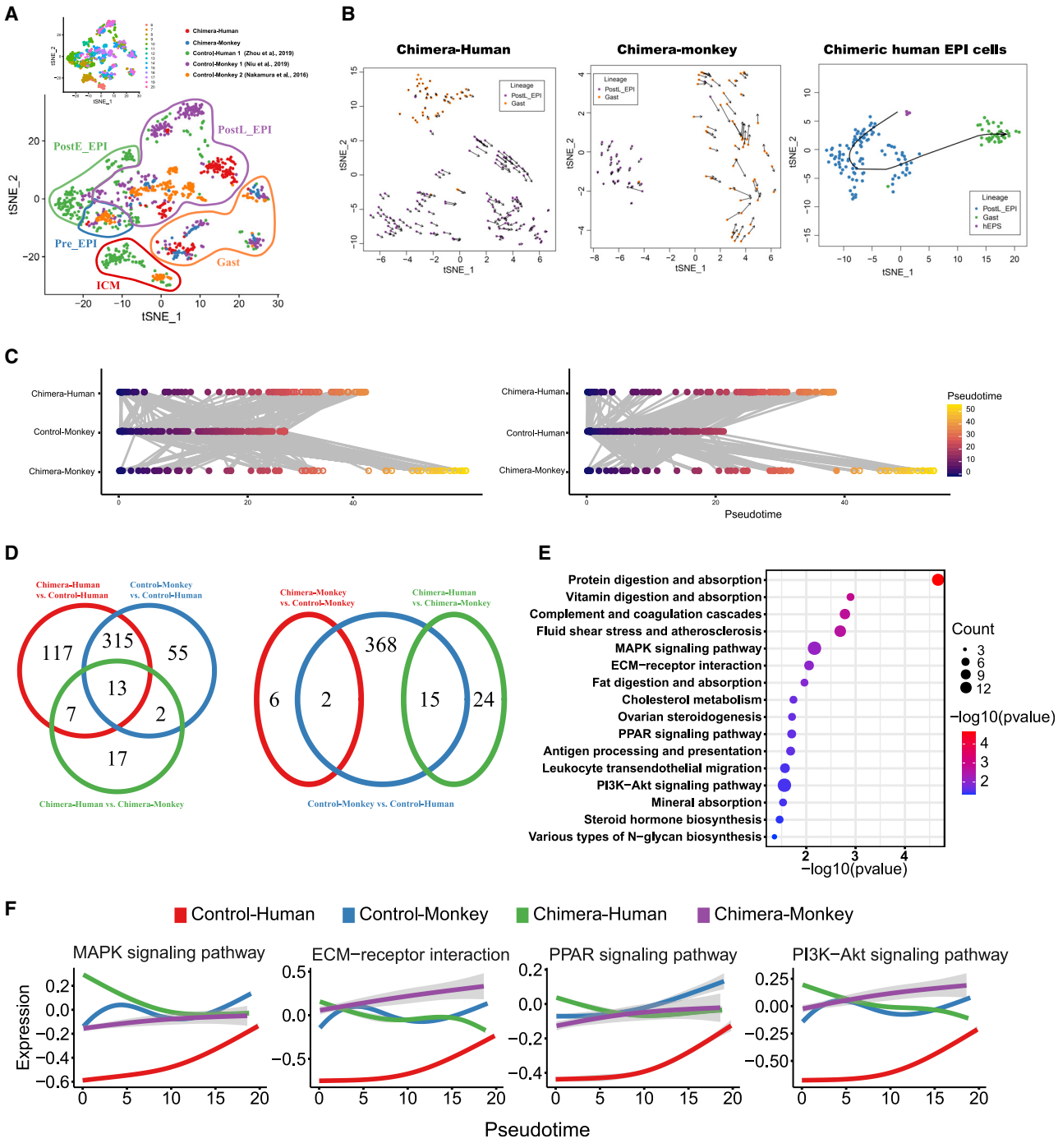

Figure 5. Developmental trajectory of chimeric human EPI-like cells within monkey embryos

(A) t-SNE plot of EPI cells at different sublineages. Cells are colored by cell origins and designated as ICM, Pre_EPI, PostE_EPI, PostL_EPI, and Gast. Cells of "Control-Human 1" derive from dataset "Human-1" (Zhou et al., 2019). Cells of "Control-Monkey 1" derive from dataset "Monkey-1" (Niu et al., 2019). Cells of "Control-Monkey 2" derive from dataset "Monkey-2" (Nakamura et al., 2016). Lower right: single cells are colored according to embryonic stages.

(B) RNA velocity analysis of chimeric human (chimera-human) and host monkey (chimera-monkey) cells, respectively (left two panels). The amplitude and direction of the vector reflects a transcriptional trajectory. Slingshot analysis of chimeric human EPI-like cells and hEPSCs (third panel). The curves and arrows indicate the potential development trajectory. Cells are colored by cell lineages.

(C) Pseudotime alignment between control and chimeric cells. Left and right panels show the pseudotime alignment of chimeric cells with control human and host monkey cells, respectively.

(legend continued on next page)

chimeric embryos than EPI cells from human embryos. To further delineate the potential processes regulating the development of chimeric human EPI-like cells, we generated Venn diagrams using DEGs identified between human EPI-like and monkey EPI cells within the chimeric embryos, between EPI cells from control human and monkey embryos, between human EPI-like cells from chimeric embryos and EPI cells from human embryos, and between EPI cells from chimeric and control monkey embryos. These analyses revealed 315 genes uniquely shared between chimeric human EPI-like cells and EPI cells from control monkey embryos (Figure 5D; Table S4). KEGG analysis using these genes identified PI3K-Akt, MAPK, and Peroxisome proliferator-activated receptor (PPAR) signaling pathways, which may be involved in shifting the transcriptomes of human EPI-like cells toward the monkey EPI cells (Figures 5E and 5F). We also found a number of hub genes that potentially played important roles in regulating the development of chimeric human EPI-like cells, namely CHD2, POLR2A, and RB1 (Figures S5A and S5B). In addition, we found that a majority of chimeric human EPI-like cells expressed S/G2/M cell-cycle-related genes, and the expression levels of apoptosis-related genes showed no significant difference among human and monkey cells within chimeric and control embryos (Figures S5C and S5E). Although chimeric human EPI-like cells showed slower than normal differentiation, GO analysis using DEGs in Pre_EPI, PostL_EPI, and gastrulating (Gast) cells revealed developmental progression (Figure S5D). Together, these analyses reveal signaling pathways and factors that likely drive distinct lineage specification and differentiation dynamics of chimeric human EPI-like cells within monkey embryos.

DISCUSSION

There are significant ethical considerations involved in generating and studying human-animal chimeric embryos, particularly when non-human primates are involved. Different guidelines exist at the state, national, and international levels, and it is important for scientists, bioethicists, policy makers, and funding agencies to stay engaged in keeping these guidelines up to date with the relevant science as well as for the welfare of society. For the studies presented here, extensive reviews of research plans and protocols were conducted in advance. Ethical consultations and reviews were performed both at the institutional level and via outreach to non-affiliated bioethicists with experience in state and national bioethics policies regarding these matters. This thorough and detailed process helped guide our experiments, which were focused entirely on *ex vivo* chimeric embryos. Furthermore, we limited our studies to early-stage chimeric embryo development.

Using hPSCs to generate human-animal chimeric embryos provides an experimental paradigm for studying early human development and holds great potential for diverse applications in regenerative medicine as well as for producing human tissues and organs for replacement therapies. To achieve interspecies blastocyst complementation, donor PSCs must be able to contribute to chimera formation once introduced into the host embryo. Rat and mouse PSCs robustly contribute to chimera formation when introduced into mouse and rat blastocysts, respectively. To date, however, robust chimerism between species that are more evolutionarily distant has not been achieved. Several groups, including ours, have rigorously demonstrated that hPSCs inefficiently contributed to chimera formation in early mouse (E8.5–E17.5) and pig (E17–E28) embryos. Levels of chimerism were far lower than those achieved between rat and mouse (Bayerl et al., 2020; Das et al., 2020; Hu et al., 2020; Salazar-Roa et al., 2020; Theunissen et al., 2014, 2016; Wang et al., 2018; Wu et al., 2017; Yang et al., 2017b). This conclusion was reached by systematically testing the chimeric competency of human embryonic stem cells (hESCs)/induced PSCs (iPSCs) generated under different culture conditions in different laboratories. Different sex and genetic backgrounds were also tested. These results likely reflect the >90-million-year evolutionary distance between primates and rodents and between primates and ungulates. By contrast, the mouse and rat are separated by ~21 million years of evolution. Thus, more pronounced xenogeneic barriers might exist between evolutionarily distant species during early development. These barriers likely reflect differences in embryonic development (Rossant, 2018; Rossant and Tam, 2018; Wu et al., 2016) that manifest at the molecular and cellular levels as differential cell adhesion, ligand-receptor incompatibility, cell competition (Zheng et al., 2021), and differences in cell-cycle rates and developmental timing, among others. To gain insights into early human development and identify key molecular processes underlying xenogeneic barriers, it is thus imperative to study human-animal chimeras using a host species that is more closely related to humans.

Dynamic PSC states reflect the spectrum of pluripotency observed *in vivo* (Morgani et al., 2017; Riveiro and Brickman, 2020; Wu and Izpisua Belmonte, 2015). Studies in rodents have identified a number of pluripotency states (e.g., naive and primed) that exhibit different molecular and functional properties, including variable abilities to contribute to chimera formation (Wu and Izpisua Belmonte, 2015). A single mouse EPSC cultured in the LCDM condition (leukemia inhibitory factor [LIF], the GSK3 inhibitor CHIR99021, (S)-(+)-dimethindene maleate [DiM)], and minocycline hydrochloride [MiH]) can give rise to an entire adult mouse via tetraploid complementation, which is not seen with other PSCs (Yang et al., 2017b). Thus, mouse EPSCs seem to exhibit the highest chimeric capability among

(D) The Venn diagram shows the overlap of DEGs obtained from different comparisons. The 315 genes (left panel shows genes that are putatively involved in making chimeric human EPI-like cells similar to host monkey EPI cells) and two genes (right panel shows genes that are putatively involved in making host monkey EPI cells similar to control human EPI cells) are subsets from the DEGs between chimera-human and control-human cells and between chimera-monkey and control-monkey cells, respectively.
(E) Enriched KEGG pathways for the 315 DEGs.
(F) The dynamic changes of the 315 DEGs enriched pathways along the pseudotime. ICM, inner cell mass; EPI, epiblast; Pre_EPI, pre-implantation EPI; PostE_EPI, post-implantation early EPI; PostL_EPI, post-implantation late EPI; Gast, gastrulating cell; DEG, differentially expressed gene.
See also Figures S4 and S5 and Table S4.

all reported PSCs. LCDM-cultured hEPSCs also exhibit relatively higher chimera competency in E10.5 mouse conceptuses (~1%) when compared with other hPSCs (Yang et al., 2017b). To maximize the possibility of a positive outcome and to minimize the number of monkey embryos used, we chose to only focus on a well-characterized hEPSC line.

In the current study, we combined prolonged *ex vivo* monkey embryo culture with hEPSC injection to study human chimerism in a closely related non-human primate species (*Macaca fascicularis)*. We found that hEPSCs were incorporated into the developmental program of the monkey embryo until d.p.f.19. Savatier and colleagues recently found that human naive PSCs stalled in the G1 phase of the cell cycle and therefore could not contribute to chimera formation when introduced into rabbit or macaque pre-implantation embryos (Aksoy et al., 2020), which is not observed in the present study. One possible explanation for this discrepancy is that PSCs cultured in the LCDM condition may acquire features that make them more proliferative and/or better able to survive in host monkey embryos, as they did in mouse chimeras (Yang et al., 2017a, 2017b). Recent studies have also shown that human and monkey PSCs residing in an intermediate pluripotent state exhibit improved chimera contribution over naive or naive-like PSCs in pig embryos (Fu et al., 2020; Wu et al., 2017). These observations suggest that donor PSC culture conditions need to be catered to different host species to enable robust interspecies chimerism.

In the current study, we found that hEPSCs contributed to several main lineages (EPI, HYP, and EXMC) in peri- and early post-implantation monkey embryos. Despite transcriptomic differences, EPI-like cells derived from hEPSCs largely followed the specification and differentiation dynamics observed in control monkey and human embryos *ex vivo*. This suggests that EPI developmental programs are evolutionarily conserved between humans and monkeys. Recently, the ability of mouse EPSCs and hEPSCs to differentiate into trophoblasts has been called into question (Guo et al., 2020; Posfai et al., 2020; Yang et al., 2017a, 2017b). Consistent with recent observations, we found that hEPSCs rarely contributed to TE derivatives in human-monkey chimeric embryos. This may be due to clonal effect (only one hEPSC line was used in this study), species differences, and/or a lack of TE potency in hEPSCs.

Our scRNA-seq analyses revealed transcriptomic differences between cells in human-monkey chimeric embryos (both human and monkey) when compared with control human and monkey embryos (data retrieved from a publicly accessible database) (Nakamura et al., 2016; Niu et al., 2019; Xiang et al., 2020; Zhou et al., 2019). This is likely because introduced human cells impacted embryonic developmental niches within the host monkey embryos. To gain insights into the mechanisms underlying these changes, we studied cell-cell interactions and examined ligand-receptor pairing. We found that cell-cell interactions between human and monkey cells within chimeric embryos showed some distinct features when compared to controls. We also identified a number of signaling pathways that were potentially involved (e.g., MAPK and PI3K-AKT). It will be interesting to determine whether modulating these pathway activities in donor hPSCs and/or cultured embryos may improve interspecies chimerism in future studies.

Most recently, interspecies PSC co-cultures (e.g., human and rhesus macaque) have been developed to study interspecies cell competition (Zheng et al., 2021). In addition, through advances in both 2D and 3D culture systems, hPSCs have been guided to patterned structures that model post-implantation developmental processes, including amniotic sac formation, gastrulation, and neurulation (Martyn et al., 2018; Shao et al., 2017; Simunovic et al., 2019; Warmflash et al., 2014; Xue et al., 2018; Zheng et al., 2019). While these *in vitro* models are valuable in studying human pluripotent EPI cells and their derivatives, they lack extra-embryonic tissues, including trophoblast and HYP. In comparison, the human-monkey *ex vivo* model reported in this study is less accessible than *in vitro* PSC models but bears the advantage of studying human development in a conceptus context that captures the spatiotemporal dynamic cell interactions from different tissues. As research progresses, all of these different models will be invaluable and complementary to one another to help gain insights into early human development.

In summary, our findings provide insights into the cellular and molecular events that occur when human and monkey cells are mixed early during embryonic development. These results shed light on evolutionarily convergent and divergent processes during primate embryogenesis. Ultimately, this line of fundamental research will help improve human chimerism in species more evolutionarily distant that for various reasons, including social, economic, and ethical, might be more appropriate for regenerative medicine translational therapies.

Limitations of study

Despite the fact that a relatively large number of cynomolgus monkey embryos (132) were used in this study, due to the inherent randomness of chimera experiments and to account for the full range of factors that potentially affect interspecies chimerism, an expanded analysis with a larger number of monkey embryos will be needed. The constraint in the number of embryos we could utilize led to several limitations of the current study: (1) we only tested chimera competency of a hEPSC line in monkey embryos and did not study other pluripotency states from human or other species (it should be noted that monkey EPSCs have not been reported to date), (2) we did not test the effect of changing the numbers of hEPSCs injected in monkey embryos, and (3) we were not able to test different injection stages.

STAR★METHODS

Detailed methods are provided in the online version of this paper and include the following:

- KEY RESOURCES TABLE
- RESOURCE AVAILABILITY
  - Lead contact
  - Materials availability
  - Data and code availability
- EXPERIMENTAL MODEL AND SUBJECT DETAILS
  - Animals
  - Culture of human extended pluripotent stem (hEPS) cells

- Animal, stem cell, and ethical approvals
- METHOD DETAILS
  - Oocyte collection and *in vitro* fertilization
  - Microinjection of human EPS cells into monkey blastocysts and *in vitro* embryo culture
  - Human-monkey chimeric embryos culture *in vitro*
  - Single cell collection and single cell RNA-seq (scRNA-seq)
  - Immunofluorescence (IF) analysis
- QUANTIFICATION AND STATISTICAL ANALYSIS
  - Statistical analysis
  - Cell origin identification, scRNA-seq data pre-processing and quality control
  - Cell clustering, lineage identification
  - Identification of differentially expressed genes
  - Pseudotime alignment and pseudotime-dependent differentially expressed genes analysis
  - GO and KEGG pathway analysis
  - Single-cell transcription factor regulation networks construction and clustering
  - RNA velocity analysis
  - Identification of cross-talks between human and monkey cells within chimeric embryos

SUPPLEMENTAL INFORMATION

Supplemental information can be found online at https://doi.org/10.1016/j.cell.2021.03.020.

ACKNOWLEDGMENTS

Special thanks to the Stanford University Research Ethics Program for helpful discussions and feedback during the protocol review process. We would like to thank David O'Keefe for his critical reading of this manuscript and invaluable comments. This work was supported by grants from the National Key Research and Development Program (2018YFA0801400 and 2016YFA0101401), the National Natural Science Foundation of China (81760271 and 31660346), Major Basic Research Project of Science and Technology of Yunnan (2017ZF028 and 202001BC070001), Key Projects of Basic Research Program in Yunnan Province (2017FA010), High-level Talent Cultivation Support Plan of Yunnan Province and Yunnan Fundamental Research Projects (2019FB050), UCAM, and The Moxie Foundation.

AUTHOR CONTRIBUTIONS

T.T., J.W., Y.N., W.J., and J.C.I.B. designed the study and supervised all experiments. C.S. and Y.K. performed samples collection work, including superovulation, micromanipulation, and animal care. T.T., Y.Z., N.S., E.Z., H.S., W.S., H.W., Z.C., R.H.-B., L.M.M., E.N.D., W.T.B., M.S., Z.A., T.L., and C.R.E. carried out experiments or contributed critical reagents and protocols. T.T., J.W., S.D., P.Y., and R.Z. analyzed the data and performed statistical analyses. T.T., J.W., S.D., W.J., and J.C.I.B. wrote the manuscript.

DECLARATION OF INTERESTS

The authors declare no competing interests.

INCLUSION AND DIVERSITY

We worked to ensure sex balance in the selection of non-human subjects. One or more of the authors of this paper self-identifies as an underrepresented ethnic minority in science. One or more of the authors of this paper self-identifies as living with a disability. One or more of the authors of this paper received support from a program designed to increase minority representation in science. The author list of this paper includes contributors from the location where the research was conducted who participated in the data collection, design, analysis, and/or interpretation of the work.

Received: September 29, 2020
Revised: January 25, 2021
Accepted: March 9, 2021
Published: April 15, 2021

REFERENCES

Aibar, S., González-Blas, C.B., Moerman, T., Huynh-Thu, V.A., Imrichova, H., Hulselmans, G., Rambow, F., Marine, J.C., Geurts, P., Aerts, J., et al. (2017). SCENIC: single-cell regulatory network inference and clustering. Nat. Methods *14*, 1083–1086.

Aksoy, I., Rognard, C., Moulin, A., Marcy, G., Masfaraud, E., Wianny, F., Cortay, V., Bellemin-Ménard, A., Doerflinger, N., Dirheimer, M., et al. (2020). Primate naïve pluripotent stem cells stall in the G1 phase of the cell cycle and differentiate prematurely during embryo colonization. bioRxiv, 2020.2003.2027.011890.

Bayerl, J., Ayyash, M., Shani, T., Manor, Y., Gafni, O., Kalma, Y., Aguilera-Castrejon, A., Zerbib, M., Amir, H., Sheban, D., et al. (2020). Tripartite Inhibition of SRC-WNT-PKC Signalling Consolidates Human Naïve Pluripotency. bioRxiv, 2020.2005.2023.112433.

Butler, A., Hoffman, P., Smibert, P., Papalexi, E., and Satija, R. (2018). Integrating single-cell transcriptomic data across different conditions, technologies, and species. Nat. Biotechnol. *36*, 411–420.

Chan, Y.S., Göke, J., Ng, J.H., Lu, X., Gonzales, K.A., Tan, C.P., Tng, W.Q., Hong, Z.Z., Lim, Y.S., and Ng, H.H. (2013). Induction of a human pluripotent state with distinct regulatory circuitry that resembles preimplantation epiblast. Cell Stem Cell *13*, 663–675.

Chen, Y., Niu, Y., Li, Y., Ai, Z., Kang, Y., Shi, H., Xiang, Z., Yang, Z., Tan, T., Si, W., et al. (2015). Generation of Cynomolgus Monkey Chimeric Fetuses using Embryonic Stem Cells. Cell Stem Cell *17*, 116–124.

Das, S., Koyano-Nakagawa, N., Gafni, O., Maeng, G., Singh, B.N., Rasmussen, T., Pan, X., Choi, K.D., Mickelson, D., Gong, W., et al. (2020). Generation of human endothelium in pig embryos deficient in ETV2. Nat. Biotechnol. *38*, 297–302.

De Los Angeles, A. (2019). The Pluripotency Continuum and Interspecies Chimeras. Curr. Protoc. Stem Cell Biol. *50*, e87.

De Los Angeles, A., Ferrari, F., Xi, R., Fujiwara, Y., Benvenisty, N., Deng, H., Hochedlinger, K., Jaenisch, R., Lee, S., Leitch, H.G., et al. (2015). Hallmarks of pluripotency. Nature *525*, 469–478.

Deglincerti, A., Croft, G.F., Pietila, L.N., Zernicka-Goetz, M., Siggia, E.D., and Brivanlou, A.H. (2016). Self-organization of the in vitro attached human embryo. Nature *533*, 251–254.

Fu, R., Yu, D., Ren, J., Li, C., Wang, J., Feng, G., Wang, X., Wan, H., Li, T., Wang, L., et al. (2020). Domesticated cynomolgus monkey embryonic stem cells allow the generation of neonatal interspecies chimeric pigs. Protein Cell *11*, 97–107.

Gafni, O., Weinberger, L., Mansour, A.A., Manor, Y.S., Chomsky, E., Ben-Yosef, D., Kalma, Y., Viukov, S., Maza, I., Zviran, A., et al. (2013). Derivation of novel human ground state naive pluripotent stem cells. Nature *504*, 282–286.

Gao, X., Nowak-Imialek, M., Chen, X., Chen, D., Herrmann, D., Ruan, D., Chen, A.C.H., Eckersley-Maslin, M.A., Ahmad, S., Lee, Y.L., et al. (2019). Establishment of porcine and human expanded potential stem cells. Nat. Cell Biol. *21*, 687–699.

Guo, G., Stirparo, G.G., Strawbridge, S., Yang, J., Clarke, J., Li, M.A., Myers, S., Özel, B.N., Nichols, J., and Smith, A. (2020). Trophectoderm Potency is Retained Exclusively in Human Naïve Cells. bioRxiv, 2020.2002.2004.933812.

Hackett, J.A., and Surani, M.A. (2014). Regulatory principles of pluripotency: from the ground state up. Cell Stem Cell *15*, 416–430.

Harvey, A., Caretti, G., Moresi, V., Renzini, A., and Adamo, S. (2019). Interplay between Metabolites and the Epigenome in Regulating Embryonic and Adult Stem Cell Potency and Maintenance. Stem Cell Reports *13*, 573–589.

Hu, Z., Li, H., Jiang, H., Ren, Y., Yu, X., Qiu, J., Stablewski, A.B., Zhang, B., Buck, M.J., and Feng, J. (2020). Transient inhibition of mTOR in human pluripotent stem cells enables robust formation of mouse-human chimeric embryos. Sci. Adv. *6*, eaaz0298.

Huang, K., Zhu, Y., Ma, Y., Zhao, B., Fan, N., Li, Y., Song, H., Chu, S., Ouyang, Z., Zhang, Q., et al. (2018). BMI1 enables interspecies chimerism with human pluripotent stem cells. Nat. Commun. *9*, 4649.

Kanehisa, M. (2019). Toward understanding the origin and evolution of cellular organisms. Protein Sci. *28*, 1947–1951.

Kanehisa, M., and Goto, S. (2000). KEGG: kyoto encyclopedia of genes and genomes. Nucleic Acids Res. *28*, 27–30.

Kanehisa, M., Sato, Y., Furumichi, M., Morishima, K., and Tanabe, M. (2019). New approach for understanding genome variations in KEGG. Nucleic Acids Res. *47* (D1), D590–D595.

Kanton, S., Boyle, M.J., He, Z., Santel, M., Weigert, A., Sanchís-Calleja, F., Guijarro, P., Sidow, L., Fleck, J.S., Han, D., et al. (2019). Organoid single-cell genomic atlas uncovers human-specific features of brain development. Nature *574*, 418–422.

Kim, D., Paggi, J.M., Park, C., Bennett, C., and Salzberg, S.L. (2019). Graph-based genome alignment and genotyping with HISAT2 and HISAT-genotype. Nat. Biotechnol. *37*, 907–915.

Kumar, S., Stecher, G., Li, M., Knyaz, C., and Tamura, K. (2018). MEGA X: Molecular Evolutionary Genetics Analysis across Computing Platforms. Mol. Biol. Evol. *35*, 1547–1549.

La Manno, G., Soldatov, R., Zeisel, A., Braun, E., Hochgerner, H., Petukhov, V., Lidschreiber, K., Kastriti, M.E., Lönnerberg, P., Furlan, A., et al. (2018). RNA velocity of single cells. Nature *560*, 494–498.

Ma, H., Zhai, J., Wan, H., Jiang, X., Wang, X., Wang, L., Xiang, Y., He, X., Zhao, Z.A., Zhao, B., et al. (2019). In vitro culture of cynomolgus monkey embryos beyond early gastrulation. Science *366*, eaax7890.

Martyn, I., Kanno, T.Y., Ruzo, A., Siggia, E.D., and Brivanlou, A.H. (2018). Self-organization of a human organizer by combined Wnt and Nodal signalling. Nature *558*, 132–135.

Mishra, R., Grzybek, M., Niki, T., Hirashima, M., and Simons, K. (2010). Galectin-9 trafficking regulates apical-basal polarity in Madin-Darby canine kidney epithelial cells. Proc. Natl. Acad. Sci. USA *107*, 17633–17638.

Morgani, S., Nichols, J., and Hadjantonakis, A.K. (2017). The many faces of Pluripotency: in vitro adaptations of a continuum of in vivo states. BMC Dev. Biol. *17*, 7.

Nakamura, T., Okamoto, I., Sasaki, K., Yabuta, Y., Iwatani, C., Tsuchiya, H., Seita, Y., Nakamura, S., Yamamoto, T., and Saitou, M. (2016). A developmental coordinate of pluripotency among mice, monkeys and humans. Nature *537*, 57–62.

Niu, Y., Sun, N., Li, C., Lei, Y., Huang, Z., Wu, J., Si, C., Dai, X., Liu, C., Wei, J., et al. (2019). Dissecting primate early post-implantation development using long-term in vitro embryo culture. Science *366*, eaaw5754.

Pertea, M., Pertea, G.M., Antonescu, C.M., Chang, T.C., Mendell, J.T., and Salzberg, S.L. (2015). StringTie enables improved reconstruction of a transcriptome from RNA-seq reads. Nat. Biotechnol. *33*, 290–295.

Picelli, S., Faridani, O.R., Björklund, A.K., Winberg, G., Sagasser, S., and Sandberg, R. (2014). Full-length RNA-seq from single cells using Smart-seq2. Nat. Protoc. *9*, 171–181.

Posfai, E., Schell, J.P., Janiszewski, A., Rovic, I., Murray, A., Bradshaw, B., Pardon, T., El Bakkali, M., Talon, I., De Geest, N., et al. (2020). Defining totipotency using criteria of increasing stringency. bioRxiv, 2020.2003.2002.972893.

Riveiro, A.R., and Brickman, J.M. (2020). From pluripotency to totipotency: an experimentalist's guide to cellular potency. Development *147*, dev189845.

Rossant, J. (2018). Genetic Control of Early Cell Lineages in the Mammalian Embryo. Annu. Rev. Genet. *52*, 185–201.

Rossant, J., and Tam, P.P.L. (2017). New Insights into Early Human Development: Lessons for Stem Cell Derivation and Differentiation. Cell Stem Cell *20*, 18–28.

Rossant, J., and Tam, P.P.L. (2018). Exploring early human embryo development. Science *360*, 1075–1076.

Salazar-Roa, M., Trakala, M., Álvarez-Fernández, M., Valdés-Mora, F., Zhong, C., Muñoz, J., Yu, Y., Peters, T.J., Graña-Castro, O., Serrano, R., et al. (2020). Transient exposure to miR-203 enhances the differentiation capacity of established pluripotent stem cells. EMBO J. *39*, e104324.

Shahbazi, M.N., Jedrusik, A., Vuoristo, S., Recher, G., Hupalowska, A., Bolton, V., Fogarty, N.N.M., Campbell, A., Devito, L., Ilic, D., et al. (2016). Self-organization of the human embryo in the absence of maternal tissues. Nat. Cell Biol. *18*, 700–708.

Shao, Y., Taniguchi, K., Townshend, R.F., Miki, T., Gumucio, D.L., and Fu, J. (2017). A pluripotent stem cell-based model for post-implantation human amniotic sac development. Nat. Commun. *8*, 208.

Simunovic, M., Metzger, J.J., Etoc, F., Yoney, A., Ruzo, A., Martyn, I., Croft, G., You, D.S., Brivanlou, A.H., and Siggia, E.D. (2019). A 3D model of a human epiblast reveals BMP4-driven symmetry breaking. Nat. Cell Biol. *21*, 900–910.

Smith, A. (2017). Formative pluripotency: the executive phase in a developmental continuum. Development *144*, 365–373.

Street, K., Risso, D., Fletcher, R.B., Das, D., Ngai, J., Yosef, N., Purdom, E., and Dudoit, S. (2018). Slingshot: cell lineage and pseudotime inference for single-cell transcriptomics. BMC Genomics *19*, 477.

Stuart, T., Butler, A., Hoffman, P., Hafemeister, C., Papalexi, E., Mauck, W.M., 3rd, Hao, Y., Stoeckius, M., Smibert, P., and Satija, R. (2019). Comprehensive Integration of Single-Cell Data. Cell *177*, 1888–1902.e1821.

Suchy, F., and Nakauchi, H. (2018). Interspecies chimeras. Curr. Opin. Genet. Dev. *52*, 36–41.

Theunissen, T.W., Powell, B.E., Wang, H., Mitalipova, M., Faddah, D.A., Reddy, J., Fan, Z.P., Maetzel, D., Ganz, K., Shi, L., et al. (2014). Systematic identification of culture conditions for induction and maintenance of naive human pluripotency. Cell Stem Cell *15*, 471–487.

Theunissen, T.W., Friedli, M., He, Y., Planet, E., O'Neil, R.C., Markoulaki, S., Pontis, J., Wang, H., Iouranova, A., Imbeault, M., et al. (2016). Molecular Criteria for Defining the Naive Human Pluripotent State. Cell Stem Cell *19*, 502–515.

Trapnell, C., Cacchiarelli, D., Grimsby, J., Pokharel, P., Li, S., Morse, M., Lennon, N.J., Livak, K.J., Mikkelsen, T.S., and Rinn, J.L. (2014). The dynamics and regulators of cell fate decisions are revealed by pseudotemporal ordering of single cells. Nat. Biotechnol. *32*, 381–386.

Vento-Tormo, R., Efremova, M., Botting, R.A., Turco, M.Y., Vento-Tormo, M., Meyer, K.B., Park, J.E., Stephenson, E., Polański, K., Goncalves, A., et al. (2018). Single-cell reconstruction of the early maternal-fetal interface in humans. Nature *563*, 347–353.

Vincent, S.D., Dunn, N.R., Hayashi, S., Norris, D.P., and Robertson, E.J. (2003). Cell fate decisions within the mouse organizer are governed by graded Nodal signals. Genes Dev. *17*, 1646–1662.

Wang, X., Li, T., Cui, T., Yu, D., Liu, C., Jiang, L., Feng, G., Wang, L., Fu, R., Zhang, X., et al. (2018). Human embryonic stem cells contribute to embryonic and extraembryonic lineages in mouse embryos upon inhibition of apoptosis. Cell Res. *28*, 126–129.

Warmflash, A., Sorre, B., Etoc, F., Siggia, E.D., and Brivanlou, A.H. (2014). A method to recapitulate early embryonic spatial patterning in human embryonic stem cells. Nat. Methods *11*, 847–854.

Weinberger, L., Ayyash, M., Novershtern, N., and Hanna, J.H. (2016). Dynamic stem cell states: naive to primed pluripotency in rodents and humans. Nat. Rev. Mol. Cell Biol. *17*, 155–169.

Weinreb, C., Wolock, S., and Klein, A.M. (2018). SPRING: a kinetic interface for visualizing high dimensional single-cell expression data. Bioinformatics *34*, 1246–1248.

Wu, J., and Izpisua Belmonte, J.C. (2015). Dynamic Pluripotent Stem Cell States and Their Applications. Cell Stem Cell *17*, 509–525.

Wu, J., and Izpisua Belmonte, J.C. (2016). Stem Cells: A Renaissance in Human Biology Research. Cell *165*, 1572–1585.

Wu, J., Greely, H.T., Jaenisch, R., Nakauchi, H., Rossant, J., and Belmonte, J.C. (2016). Stem cells and interspecies chimaeras. Nature *540*, 51–59.

Wu, J., Platero-Luengo, A., Sakurai, M., Sugawara, A., Gil, M.A., Yamauchi, T., Suzuki, K., Bogliotti, Y.S., Cuello, C., Morales Valencia, M., et al. (2017). Interspecies Chimerism with Mammalian Pluripotent Stem Cells. Cell *168*, 473–486.e15.

Xiang, L., Yin, Y., Zheng, Y., Ma, Y., Li, Y., Zhao, Z., Guo, J., Ai, Z., Niu, Y., Duan, K., et al. (2020). A developmental landscape of 3D-cultured human pre-gastrulation embryos. Nature *577*, 537–542.

Xue, X., Sun, Y., Resto-Irizarry, A.M., Yuan, Y., Aw Yong, K.M., Zheng, Y., Weng, S., Shao, Y., Chai, Y., Studer, L., and Fu, J. (2018). Mechanics-guided embryonic patterning of neuroectoderm tissue from human pluripotent stem cells. Nat. Mater. *17*, 633–641.

Yang, J., Ryan, D.J., Wang, W., Tsang, J.C., Lan, G., Masaki, H., Gao, X., Antunes, L., Yu, Y., Zhu, Z., et al. (2017a). Establishment of mouse expanded potential stem cells. Nature *550*, 393–397.

Yang, Y., Liu, B., Xu, J., Wang, J., Wu, J., Shi, C., Xu, Y., Dong, J., Wang, C., Lai, W., et al. (2017b). Derivation of Pluripotent Stem Cells with In Vivo Embryonic and Extraembryonic Potency. Cell *169*, 243–257.e25.

Yu, G., Wang, L.G., Han, Y., and He, Q.Y. (2012). clusterProfiler: an R package for comparing biological themes among gene clusters. OMICS *16*, 284–287.

Zhang, J., Zhao, J., Dahan, P., Lu, V., Zhang, C., Li, H., and Teitell, M.A. (2018). Metabolism in Pluripotent Stem Cells and Early Mammalian Development. Cell Metab. *27*, 332–338.

Zheng, Y., Xue, X., Shao, Y., Wang, S., Esfahani, S.N., Li, Z., Muncie, J.M., Lakins, J.N., Weaver, V.M., Gumucio, D.L., and Fu, J. (2019). Controlled modelling of human epiblast and amnion development using stem cells. Nature *573*, 421–425.

Zheng, C., Hu, Y., Sakurai, M., Pinzon-Arteaga, C.A., Li, J., Wei, Y., Okamura, D., Ravaux, B., Barlow, H.R., Yu, L., et al. (2021). Cell competition constitutes a barrier for interspecies chimerism. Nature. Published online January 28, 221. https://doi.org/10.1038/s41586-021-03273-0.

Zhou, F., Wang, R., Yuan, P., Ren, Y., Mao, Y., Li, R., Lian, Y., Li, J., Wen, L., Yan, L., et al. (2019). Reconstituting the transcriptome and DNA methylome landscapes of human implantation. Nature *572*, 660–664.

STAR★METHODS

KEY RESOURCES TABLE

REAGENT or RESOURCE	SOURCE	IDENTIFIER
Antibodies		
Oct-3/4 (C-10)	Santa Cruz Biotechnologies	Cat#sc-5279; RRID: AB_628051
NANOG	R&D systems	Cat#AF1997; RRID: AB_355097
GATA-6 (D61E4) XP Rabbit mAb	Cell Signaling Technology	Cat#5851; RRID: AB_10705521
GATA4	Abcam	Cat#Ab124265; RRID: AB_11000793
SOX17	R&D systems	Cat#AF1924; RRID: AB_355060
PDGFRa	Abcam	Cat#Ab203491
Brachyury (H-210)/T	Santa Cruz Biotechnologies	Cat#sc-20109; RRID: AB_2255702
OTX2	Santa Cruz Biotechnologies	Cat#sc-514195
AP-2γ (6E4/4)/TFAP2C	Santa Cruz Biotechnologies	Cat#sc-12762
Anti-Collagen VI antibody/COL6A1	Abcam	Cat#ab6588; RRID: AB_305585
Anti-Cytokeratin 7	Abcam	Cat#ab68459; RRID: AB_1139824
OCT3-4	R&D systems	Cat#AF1759; RRID: AB_354975
SOX2	Abcam	Cat#ab137385; RRID: AB_2814892
Donkey anti goat IgG Alexa Fluor@647	Abcam	Cat#ab150135; RRID: AB_2687955
Donkey anti goat IgG Alexa Fluor@488	Abcam	Cat#ab150129; RRID: AB_2687506
Goat Anti-Rabbit IgG H&L (Alexa Fluor 647)	Abcam	Cat#ab150079
Goat anti-Rabbit IgG (H+L) Secondary Antibody, DyLight 488	ThermoFisher	Cat#35552; RRID: AB_844398
Goat anti-Mouse IgG (H+L) Cross-Adsorbed Secondary Antibody, Alexa Fluor 647	ThermoFisher	Cat#A21235; RRID: AB_2535804
Goat anti-Mouse IgG / IgM (H+L) 488	ThermoFisher	Cat#A10680; RRID: AB_2534062
Biological samples		
Macaca fascicularis embryos	State Key Laboratory of Primate Biomedical Research	N/A
Chemicals, peptides, and recombinant proteins		
Recombinant Human LIF	Peprotech	Cat#AF-300-05
CHIR 99021	Tocris	Cat#4423; CAS: 252917-06-9
Y-27632 dihydrochloride	Tocris	Cat#1254; CAS: 129830-38-2
(S)-(+)-Dimethindene maleate	Tocris	Cat#1425; CAS: 136152-65-3
Minocycline, Hydrochloride	Selleck	Cat#S4226; CAS: 13614-98-7
IWR-1-endo	Peprotech	Cat#1128234; CAS: 1127442-82-3
KnockOut Serum Replacement	ThermoFisher	Cat#A3181502
Neurobasal Medium	ThermoFisher	Cat#21103-049
DMEM/F-12	ThermoFisher	Cat#11320-033
N-2 Supplement	ThermoFisher	Cat#17502-048
B-27 Supplement, minus vitamin A	ThermoFisher	Cat#12587-010
GlutaMAX	ThermoFisher	Cat#35050-061
Non-Essential Amino Acids Solution	ThermoFisher	Cat#11140-050
2-Mercaptoethanol	ThermoFisher	Cat#21985-023
Penicilin-Streptomycin	ThermoFisher	Cat#15140-122
Mitomycin C from Streptomyces caespitosus	Sigma-Aldrich	Cat#M4287; CAS: 50-07-7

(*Continued on next page*)

Continued

REAGENT or RESOURCE	SOURCE	IDENTIFIER
Trypsin-EDTA (0.05%), phenol red	ThermoFisher	Cat#25300-062
DMEM-Dulbecco's Modified Eagle Medium, High Glucose	ThermoFisher	Cat#11965092
TrypLE Express Enzyme (1X), no phenol red	ThermoFisher	Cat#12604021
heat-inactivated FBS	Corning	Cat#35-076-CV
L-glutamine, 100 ×	ThermoFisher	Cat#25030
Insulin-Transferrin-Selenium-Ethanolamine (ITS -X) (100X)	ThermoFisher	Cat#51500-056
β-estradiol	Sigma-Aldrich	Cat#E8875; CAS: 50-28-2
N-acetyl- L-cysteine	Sigma-Aldrich	Cat#A7250; CAS: 616-91-1
Progesterone	Sigma-Aldrich	Cat#P0130; CAS: 57-83-0
KnockOut Serum Replacement	ThermoFisher	Cat#10828010
4',6-diamidino-2-phenylindole (DAPI)	Sigma-Aldrich	Cat# D9542CAS: 28718-90-3
Recombinant human follitropin alpha	Merck Serono	GONAL-F
Recombinant human chorionic gonadotropin alpha	Merck Serono	OVIDREL
CMRL-1066	ThermoFisher	Cat#11530037
PBS	Biological Industries	Cat#02-020-1A
4% Paraformaldehyde (PFA)	Biosharp	Cat#BL539A
Sucrose	meilunbio	Cat# BGC005CAS:57-50-1
optimal cutting temperature compound (Tissue-Tek OCT)	SAKURA	Cat#4583
FBS	Biological Industries	Cat# 04-001-1A
BSA	Sigma-Aldrich	Cat#B2064CAS: 9048-46-8
PBS	Meilunbio	Cat#MA0008
Trypsin-EDTA (0.25%), phenol red	Thermo Fisher	Cat#25200-072
Triton X-100	Sigma-Aldrich	Cat#T9284; CAS: 9002-93-1
FBS	Biological Industries	Cat# 04-002-1A
Critical commercial assays		
Superscript II reverse transcriptase	Invitrogen	Cat#18064-014
KAPA HiFi HotStart ReadyMix	KAPA Biosystems	Cat#KK2601
Betaine	Sigma-Aldrich	Cat#61962; CAS: 107-43-7
Triton X-100	Sigma-Aldrich	Cat#T9284; CAS: 9002-93-1
Magnesium chloride	Sigma-Aldrich	Cat#M8266; CAS: 7786-30-3
EB solution	QIAGEN	Cat#19086
dNTP mix	TAKARA	Cat#4030Q
Recombinant RNase inhibitor	TAKARA	Cat#2313A
RNase-OFF	TAKARA	Cat#9037
Agencourt Ampure XP beads	Beckman Coulter	Cat#A63881
HiSeq X Ten Reagent Kit v2.5	Illumina	Cat#FC-501-2521
QuBit dsDNA HS Assay Kit (used with QuBit 3.0)	Invitrogen	Cat#Q32851
TruePrep DNA Library Prep Kit V2 for Illumina	Vazyme	Cat#TD501-503
High sensitivity DNA reagents (used with Agilent Bioanalyzer 2100 system)	Agilent Technologies	Cat#5067-4626
Deposited data		
Single cell RNAseq data generated in this study	This paper	GEO: GSE155381

(*Continued on next page*)

Continued

REAGENT or RESOURCE	SOURCE	IDENTIFIER
Experimental models: cell lines		
iPS1-EPS	Yang et al., 2017	N/A
Experimental models: organisms/strains		
Macaca fascicularis	State Key Laboratory of Primate Biomedical Research	N/A
Oligonucleotides		
Oligo-dT$_{30}$VN/ISPCR oligo/TSO	TSINGKE oligo store (Picelli et al., 2014)	N/A
Software and algorithms		
HISAT2 version 2.2.1	Kim et al., 2019	https://daehwankimlab.github.io/hisat2/
StringTie version 2.1.2	Pertea et al., 2015	https://ccb.jhu.edu/software/stringtie/index.shtml
SPRING_dev	Weinreb et al., 2018	https://github.com/AllonMKlein/SPRING_dev
R package Seurat version 3.1.1	Butler et al., 2018	https://cran.r-project.org/web/packages/Seurat/index.html
R package monocle version 2.12.0	Trapnell et al., 2014	https://github.com/cole-trapnell-lab/monocle-release
R package SCENIC version 1.1.1-10	Aibar et al., 2017	https://github.com/aertslab/SCENIC
R package velocyto.R version 0.6	La Manno et al., 2018	https://github.com/velocyto-team/velocyto.R
R package clusterProfiler version 3.16.0	Yu et al., 2012	https://www.bioconductor.org/packages//2.10/bioc/html/clusterProfiler.html
CellPhoneDB version 2.0.1	Vento-Tormo et al., 2018	https://github.com/Teichlab/cellphonedb
R package slingshot version 1.1-2	Street et al., 2018	http://www.bioconductor.org/packages/release/bioc/html/slingshot.html

RESOURCE AVAILABILITY

Lead contact

Further information and requests for reagents may be directed to and will be fulfilled by Lead Contact Juan Carlos Izpisua Belmonte (belmonte@salk.edu).

Materials availability

This study did not generate any unique reagents.

Data and code availability

All sequencing data were deposited at the NCBI Gene Expression Omnibus (GEO) under accession number GSE155381.

EXPERIMENTAL MODEL AND SUBJECT DETAILS

Animals

10 healthy female cynomolgus monkeys (*Macaca fascicularis*), ranging in age from 5 to 8 years with body weights of 4 to 6 kg, were selected for use in this study. All animals were housed at the State Key Laboratory of Primate Biomedical Research (LPBR). All animal and experiment procedures were approved by the ethical committee of the LPBR and performed by following the guidelines of the Association for Assessment and Accreditation of Laboratory Animal Care International (AAALAC) for the ethical treatment of non-human primates.

Culture of human extended pluripotent stem (hEPS) cells

Human EPS cells were cultured on MEFs in serum-free N2B27-LCDM medium under 20%O2 and 5%CO2 at 37°C . The 500mL LCDM medium is composed of 240 mL DMEM/F12 (ThermoFisher Scientific, 11320-033), 240 mL Neurobasal (ThermoFisher

Scientific, 21103-049), 2.5 mL N2 supplement (ThermoFisher Scientific, 17502-048), 5 mL B27 supplement (ThermoFisher Scientific, 12587-010), 1% GlutaMAX (ThermoFisher Scientific, 35050-061), 1%non-essential amino acids (ThermoFisher Scientific, 11140-050), 0.1mM b-mercaptoethanol (ThermoFisher Scientific, 21985-023), penicillin-streptomycin (ThermoFisher Scientific, 15140-122), 5% knockout serum replacement (KSR, ThermoFisher Scientific, A3181502, optional). 10 ng/ml recombinant human LIF (L, 10ng/ml; Peprotech, AF-300-05), CHIR99021 (C, human: 1 mM, Tocris, 4423), (S)-(+)-Dimethindene maleate (D, 2 mM; Tocris, 1425), Minocycline hydrochloride (M, 2 mM; Selleck, S4226), IWR-1-endo (1 μM; Peprotech, 1128234) and Y-27632 (2 mM; Tocris, 1254). Human EPS cells were passaged by treatment with TrypLE (ThermoFisher Scientific,12604021) every 3-4 days at a split ratio of 1:10.

Animal, stem cell, and ethical approvals

At the LPBR, the animal research protocol is guided by a set of National and Provincial regulations and institutional policies. LPBR is also subject to additional standards that go beyond domestic regulatory requirements by also maintaining accreditation through the Association for Assessment and Accreditation of Laboratory Animal Care (AAALAC) International.

An original animal research protocol was drafted based on the collaborative research proposal with the Salk Institute team. After review by the executive leadership of LPBR and Institute of Primate Translational Medicine and Kunming University of Science and Technology (IPTM, KUST), the protocol was submitted to the LPBR committee and discussed at two committee meetings in Oct. 2017. After that, the animal research protocol was redrafted based on suggestions from the committee and submitted to the Institutional Animal Care and Use Committee (IACUC) of LPBR in Dec. 2017. IACUC members suggested additional edits, which were subsequently incorporated. In Jan. 2018, the protocol (LPBR201803001) received approval and was sent to the Salk Institute. The protocol was updated and approved again in 2019 and renewed in 2020. The research protocol was also submitted to the Medical Ethics Committee of LPBR in Oct. 2019 and received approval in Nov. 2019.

On the Salk Institute side, the original proposal was submitted to the Embryonic Stem Cell Research Oversight (ESCRO) committee in September 2017. The protocol was further discussed with the Salk Institute President and the executive leadership team, which recommended seeking additional external bioethical input. Members of the ESCRO review committee discussed the protocol with two renowned external bioethicists in early January 2018. Additional external outreach was made to the California Institute of Regenerative Medicine (CIRM) in February 2018 for feedback and insight on protocol review. There was no CIRM or NIH funding involved in this research.

The protocol was redrafted to incorporate requested information from the ESCRO committee, senior Salk Institute leadership, and suggestions from the external bioethicists and CIRM official. The protocol (18-0001sc) received approval Feb. 2018, and the renewal of this protocol was approved again in 2019, and again in early 2020.

METHOD DETAILS

Oocyte collection and *in vitro* fertilization

Ovarian stimulation, oocyte recovery and *in vitro* fertilization were performed as previously described (Mishra et al., 2010). In brief, healthy female cynomolgus monkeys were subjected to follicular stimulation by intramuscular injection of 20 IU of recombinant human follitropin alpha (rhFSH, Gonal F, Merck Serono) for 8 days, then 1,000 IU recombinant human chorionic gonadotropin alpha (rhCG, OVIDREL, Merck Serono) was injected on day 9. Cumulus-oocyte complexes were collected by laparoscopic follicular aspiration 32-35 hours following rhCG administration. Follicular contents were placed in HEPES-buffered Tyrode's albumin lactate pyruvate (TALP) medium containing 0.3% bovine serum albumin (BSA) at 37°C. Oocytes were stripped of cumulus cells by pipetting after a brief exposure (< 1 minute) to hyaluronidase (0.5 mg/mL) in TALP-HEPES to allow visual selection of nuclear maturity metaphase II (MII; first polar body present) oocytes. The mature oocytes were subjected to intracytoplasmic sperm injection (ICSI) immediately and then cultured in CMRL-1066 medium (GIBCO, 11530037) containing 10% fetal bovine serum (FBS, GIBCO) at 37°C in 5% CO_2. Fertilization was confirmed by the presence of the second polar body and two pronuclei. Zygotes were then cultured in the chemically defined hamster embryo culture medium-9 (HECM-9) containing 10% fetal bovine serum at 37°C in 5% CO_2 to allow embryo development. All chemicals were from Sigma Chemicals unless otherwise stated.

Microinjection of human EPS cells into monkey blastocysts and *in vitro* embryo culture

Blastocysts at day 6 of post-fertilization (early stage blastocyst) were transferred into a 50 μL manipulation droplet of TH3 in the center of a Petri dish covered with 3 mL of mineral oil. A previously established and well-characterized hEPS cell line generated by cellular reprogramming iPS1-EPS, was used for cell microinjection (Yang et al., 2017b). Single cell suspensions of hEPS cells were placed into a separate 10 uL droplet of culture medium next to the manipulation drop. 25 single tdTomato positive hEPS cells were aspirated into a 15 μm inside diameter injection pipette with 30 degrees oblique mouth. The blastocyst was held with a holding pipette and the injection pipette was moved to the manipulation droplet. Meanwhile, the zona pellucida was ablated using a single laser pulse, and the injection pipette containing hEPS cells was immediately inserted into the hole in the blastocyst, close to the ICM. Injected blastocysts were quickly transferred into the mixed media of HECM-9 and hEPS cell culture media (1:1) (Yang et al., 2017b), and cultured for 24 hours to the well-expanded blastocyst stage.

Human-monkey chimeric embryos culture *in vitro*

The tdTomato positive human-monkey chimeric embryos were selected for follow-up experiments. Generally, the zona pellucida of the human-monkey chimeric embryo was removed by exposure to hyaluronidase from bovine testes for about 30 s, and then the embryos were seeded in 8-well μ-plates (80826, Ibidi) with pre-equilibrated *in vitro* culture medium 1 (IVC1). After the embryos attached to the well, half of the IVC1 medium was exchanged with *in vitro* culture medium 2 (IVC2). Thereafter, half of the medium was replaced daily with fresh IVC2, and monkey embryos were harvested at the indicated day. Embryo culture was performed at 37°C in 5% CO_2. The ingredients of IVC1 and IVC2 were published before (Niu et al., 2019).

IVC1: DMEM/F12 (11320-033, Thermo Fisher Scientific) supplemented with 20% (vol/vol) heat-inactivated FBS (35-076-CV, Corning), 2mM L-glutamine (25030; Thermo Fisher Scientific), Penicillin (25units/ml)/streptomycin (25μg/ml) (15140-122; ThermoFisher Scientific), 1X ITS-X (51500-056; ThermoFisher Scientific), 8nM β-estradiol, 200ng/ml progesterone and 25μM N-acetyl- L-cysteine.

IVC2: 20% (vol/vol) heat-inactivated FBS of IVC1 was replaced with 30% (vol/vol) KnockOut Serum Replacement (KoSR, 10828010, Thermo Fisher Scientific).

Single cell collection and single cell RNA-seq (scRNA-seq)

After washing with phosphate buffered saline (PBS) (MA0008, meilunbio), the embryo was cut into several pieces with a 1mL syringe. The tdTomato positive and negative pieces were picked under fluorescence microscope (Leica), and digested into single cells with 0.1% trypsin (25200-072, GIBCO) at 37°C for 3 to 5 minutes. After neutralization with 2% FBS (04-002-1A, Biological Industries), cells were washed with cold PBS containing 0.1 to 1% BSA. Finally, individual tdTomato positive and negative cells were picked into a lysis buffer on ice with a mouth pipette using a fluorescence microscope.

For scRNA-seq, the cDNA synthesis, amplification and library construction of single-cell were performed according to Smart-seq2 protocol (Picelli et al., 2014). Briefly, the single-cell was placed into the lysis buffer by a mouth pipette. The reverse transcription reaction and pre-amplification were performed using SuperScript II (18064-071,Invitrogen), and KAPA HiFi HotStart Ready Mix (KK2602, KAPA Biostems), respectively. Then 20 cycles of PCR were applied to obtain ~20-140 ng of amplified cDNA. For library construction, the cDNA was fragmented by Tn5 transposase (TD502/TD501, Vazyme) mixed at 55°C for 10 minutes and followed by PCR amplification using TruePrep Amplify Enzyme (TD601, Vazyme). Then the libraries were purified and size selected with AMPure XP magnetic beads (A63881, Beckman Coulter). All libraries were adapted for sequencing on an Illumina X-Ten platform (sequenced by Annorad).

Immunofluorescence (IF) analysis

The IF analysis was conducted similarly to what was previously published (Niu et al., 2019). Human-monkey chimeric embryos cultured *in vitro* were harvested and fixed in 4% (w/v) paraformaldehyde (BL539A , Biosharp) in PBS for 30 minutes at room temperature and washed with PBS. The d.p.f.9 embryos were stained directly and the embryos from d.p.f.11 to 19 were dehydrated in sucrose (BGC005, meilunbio) solutions each for 6 hours with increasing concentration from 15% (w/v) to 30% (w/v). After embedding in optimal cutting temperature compound (4583, Tissue-Tek OCT, SAKURA), and frozen at −80°C, the embryos were prepared as cryosections with 8 μm thickness on pre-treated glass slides (1A5105, CITOTEST), and air-dried for 1 hour. After being permeabilized in PBST (PBS with 0.3% Triton X-100) (T9284, Sigma-Aldrich) for 30 minutes at room temperature, samples were blocked with 3% (w/v) BSA and 10% (v/v) FBS (04-001-1A, Biological Industries) in PBS overnight at 4°C. Slides were then incubated with primary antibodies (Table S1) overnight at 4°C. After washing at least three times, fluorescence-conjugated secondary antibodies (Table S1), and 4',6-diamidino-2-phenylindole (DAPI) were incubated with the slides in the dark at room temperature for 2 hours. Images were taken using a Leica TCS SP8 confocal microscope.

QUANTIFICATION AND STATISTICAL ANALYSIS

Statistical analysis

All values are depicted as mean ± SD. Statistical parameters including statistical analysis, statistical significance, and n value are reported in the Figure legends and Supplementary Figure legends. Statistical analyses were performed using Prism Software (GraphPad). For statistical comparison, one-way ANOVA was employed. A value of $p < 0.05$ was considered significant.

Cell origin identification, scRNA-seq data pre-processing and quality control

First, human and monkey cells were identified by two different methodologies using clean data. One was to compare the number of identical hits of sequencing reads from each cell by blastp with the randomly selected 10000 reads against the human or monkey genome (Ensembl Homo_sapiens.GRCh38 and Macaca_fascicularis_5.0), respectively. Another was to compare the read counts of sequencing reads mapped to the tdTomato sequence. After identification of cell origin, hisat2 (Kim et al., 2019) was used to map sequencing reads to the human or monkey genome with the default parameters. The program StringTie (Pertea et al., 2015) with default parameters was used to assemble alignments into potential transcripts and quantify the gene expression as transcripts

per million mapped reads (TPM) value. The cells with mapped rate > = 30% and more than 2000 genes with TPM value > 0 were processed for further analyses.

Cell clustering, lineage identification

The Seurat package (v.3.1.1) (Butler et al., 2018) was used to perform single-cell clustering analysis and t-distributed stochastic neighbor embedding (t-SNE) was applied to visualize the results. In order to identify and compare the cluster, the known lineages from previous studies were used as a reference. The reference datasets include Human-1 (Zhou et al., 2019), Human-2 (Xiang et al., 2020), monkey-1 (Niu et al., 2019) and monkey-2 (Nakamura et al., 2016). The reference dataset of Control-monkey is monkey-1 unless otherwise stated. The chimera data in our study were integrated into the above reference datasets following the below steps. First, these datasets were created as Seurat object, respectively, with the order of Human-1, Human-2, monkey-1, chimera-human and chimera-monkey. Then ''FindIntegrationAnchors'' function took these objects as input with parameters as ''k.anchor = 5, anchor.features = 2000'' and returned an anchor object. Finally, ''IntegrateData'' function used the anchor object to integrate all datasets with the default parameter. The top-20 principal components (PCs) were used for clustering (with a resolution of 0.6) by Seurat. Each cluster was defined by specific marker genes highlighted on the t-SNE graph using the ''FeaturePlot'' function and confirmed by known lineages from previous studies.

Identification of differentially expressed genes

Unique cluster-specific expressed genes were identified by running the Seurat ''FindAllMarkers'' and ''FindClusters'' functions ($p < 0.01$). The K-nearest neighbor algorithm SPRING (Weinreb et al., 2018) was used for trajectory analyses with the integrated data, 2000 highly variable genes (HVGs) and default parameters as input. To build the phylogenetic tree of all chimeric cells, the pairwise euclidean distance calculated from integrated expression matrix was fed into MEGA (X 10.1) (Kumar et al., 2018) to build the NJ tree under the phylogeny menu.

Pseudotime alignment and pseudotime-dependent differentially expressed genes analysis

The Monocle2 (v2.12.0) (Trapnell et al., 2014) was used to construct the pseudotime course of all EPI cells. The 2000 HVGs and expression data of human, monkey, and chimeric cells in the EPI lineage identified above separately was used as input for Monocle2. Dimensionalities were reduced by the ''reduceDimension'' function with the parameter ''max_components=2.'' After projecting the expression data into a lower-dimensional space, cells were ordered by performing the ''orderCells'' function. Finally, we used a dynamic time warping (DTW) algorithm to align different pseudotime courses among human, monkey, and chimeric cells as described in the previous study (Kanton et al., 2019). After pseudotime alignment, we used an F-test-based ANOVA analysis to identify genes with pseudotime-dependent expression patterns as described previously (Kanton et al., 2019). In brief, for each HVG, we established a natural splined linear regression model (ns function in the R package splines) with six degrees of freedom (df), with expression levels as the response variable and pseudotimes as the independent variable. Then an F-test was applied to compare the variation explained by the splined linear model with that of the residuals normalized by degrees of freedom. Bonferroni correction was performed across tested genes, with a corrected P value threshold of 0.01 to identify genes with pseudotime-dependent expression. In addition, the R package slingshot (v1.1-2) was used to infer the potential development trajectory of chimeric human EPI-like cells and hEPS with default settings (Street et al., 2018).

GO and KEGG pathway analysis

We used the functions enrichKEGG and enrichGO in clusterProfiler R package (Yu et al., 2012) to perform KEGG pathways (Kanehisa, 2019; Kanehisa and Goto, 2000; Kanehisa et al., 2019) and Gene Ontology (GO) biological processes enrichment analysis. A pathway or process with a P value ≤ 0.05 was considered to be significantly enriched. The enriched pathways and processes were visualized with the ''ggplot'' function in the ggplot2 package in R.

Single-cell transcription factor regulation networks construction and clustering

The SCENIC package (Aibar et al., 2017) was applied to infer and characterize the gene regulation networks (regulon) for our scRNA-seq data of chimeric cells. Based on the manual from the website (https://github.com/aertslab/SCENIC), three main steps were executed: 1. Co-expression networks between transcription factors and the potential target genes inference based on the embedded GENIE3 package; 2. For each co-expression module, the cis-regulatory motif enrichment analysis was performed among all potential target genes by RcisTarget. Each transcription factor and its direct target genes were defined as a regulon; and 3. The activity score of each regulon in each cell was computed through AUCell packages. Here, we fed the transcriptome profile of all chimeric cells to SCENIC to infer their AUC regulon activity. Then, chimeric cells were cluster based on their regulon activity with the ''pheatmap'' function in the pheatmap package (v1.0.10). For comparison, the above datasets Human-1 and monkey-1 were also performed using the same analysis of regulon activity.

RNA velocity analysis

RNA velocity was calculated using the Velocyto.R program (http://velocyto.org) on the basis of spliced and unspliced transcript reads as previously reported (La Manno et al., 2018). At first, Velocyto used a BAM file to count spliced and unspliced reads, and generated

the loom file. Those loom files were then loaded into R using the 'read.loom.matrices' function to generate count tables for splicing and unsplicing reads. RNA velocity was estimated using a gene-relative model with k-nearest neighbor cell pooling (kCells = 10). For other parameters, we used the standard R implementation of velocyto with default settings.

Identification of cross-talks between human and monkey cells within chimeric embryos

The signaling cross-talks between human and monkey cells in different embryonic lineages were built based on the ligand-receptor interactions using CellPhoneDB (v2.0.1) (Vento-Tormo et al., 2018). All the ligand-receptor interaction databases that integrated into CellPhoneDB were used for our data analysis. Here we fed the transcriptome profile of all chimeric cells and their information including cell type (human or monkey cell) and lineages information (EPI, HYP, and EXMC) to CellPhoneDB to infer potential interaction between two types of cells. An adjusted P value of 0.05 from a Permutation test was used as a threshold to identify ligands/receptors specifically expressed between two types of cells. The other parameters were set as default. For comparison, the above datasets Human-1 and monkey-1 were also used to perform the same analysis of ligand-receptor interactions.

CellPress

Supplemental figures

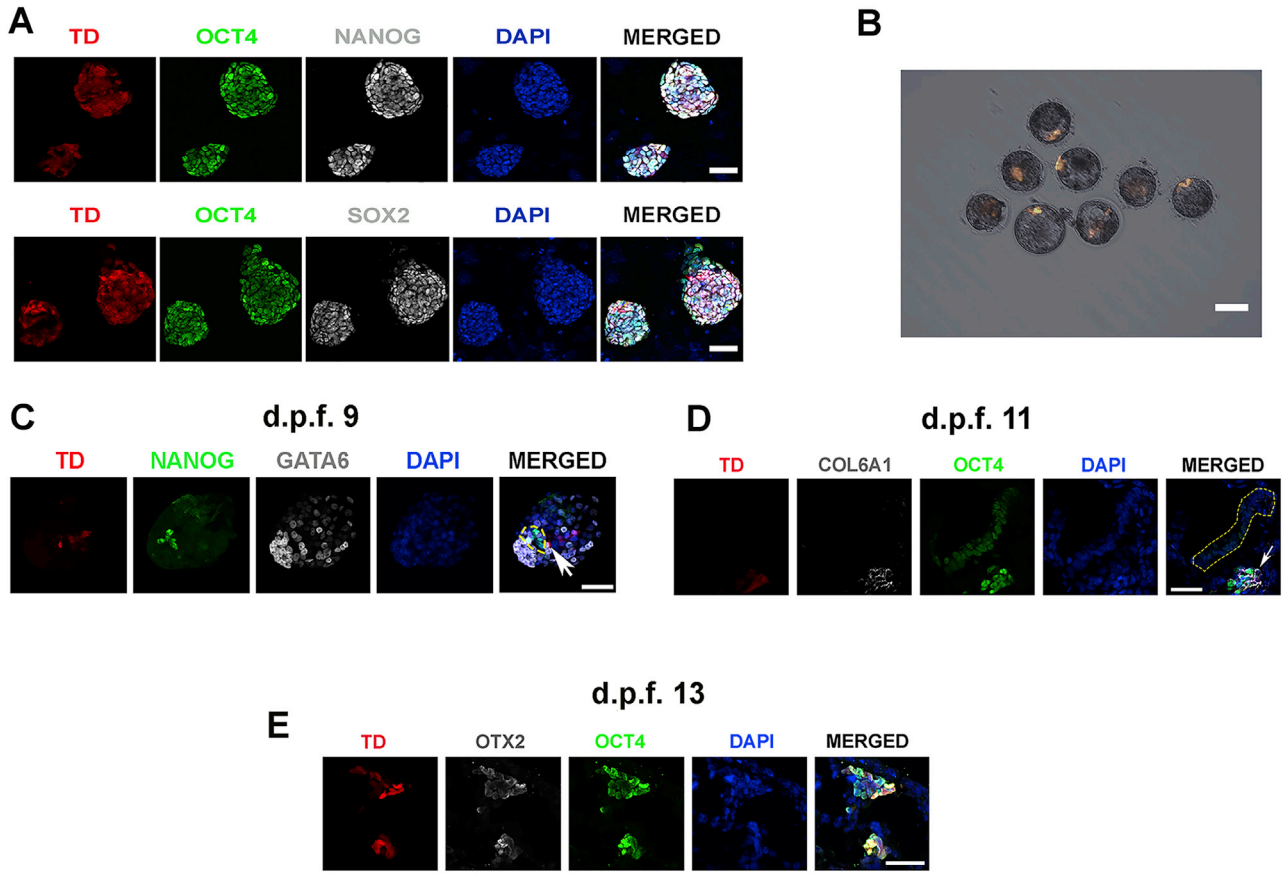

Figure S1. Lineage specification of hEPSCs within host monkey embryos, related to Figures 1 and 2

(A) Representative IF images of OCT4 (green), NANOG (gray) or SOX2 (gray) in iPS1-hEPSCs. Scale bars, 50 μm.

(B) Representative epifluorescence images of the late blastocyst-stage monkey host embryos resulting from microinjection of 25 TD-positive iPS1-hEPSCs. Scale bar, 50 μm.

(C) Representative IF images of NANOG (green) and GATA6 (gray) in d.p.f. 9 (n = 2) monkey embryos. Yellow dotted line, ICM. Arrow indicates a TD-positive hEPSC close to NANOG positive cells. Scale bar, 50 μm.

(D) Representative IF images of OCT4 (green) and COL6A1 (gray) in d.p.f. 11 monkey embryos (n = 2). Yellow dotted line, EPI. Arrow indicates a TD-positive hEPSC expressing COL6A1 and OCT4. Scale bar, 50 μm.

(E) Representative IF images OTX2 (gray) and OCT4 (green) in d.p.f.13 monkey embryos (n = 2) . Scale bar, 50 μm. EPI, epiblast; TD, tdTomato; DAPI, 4',6-diamidino-2-phenylindole.

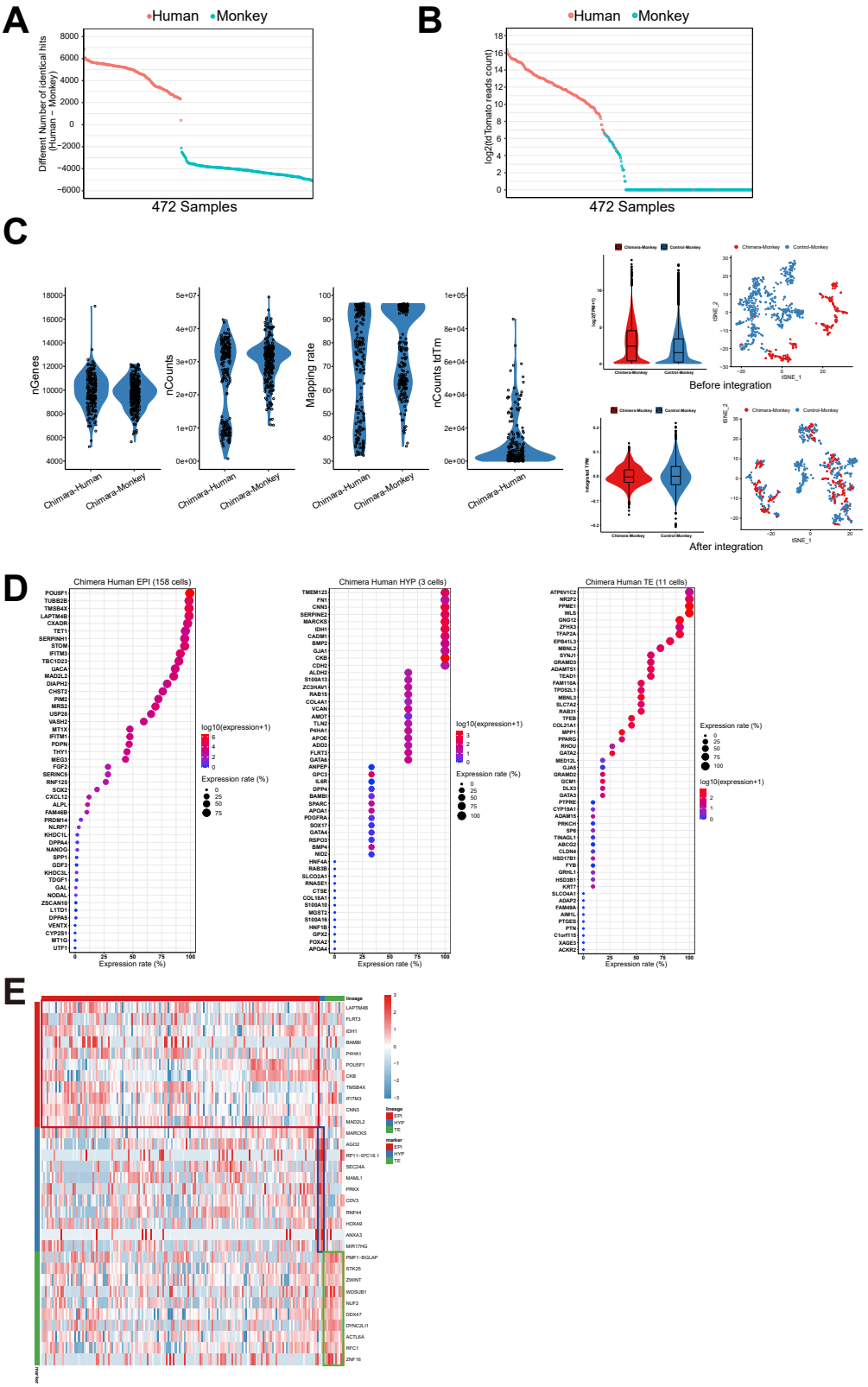

(legend on next page)

Figure S2. Identification of cell species origin and quality control, related to Figure 3

(A and B) Both the different number of identical hits by blastp (A) and tdTomato reads (B) can distinguish the cell origin. Red and green points represent cell samples from human or monkey, respectively.

(C) The quality control and statistic analysis of gene numbers (nGene) and reads numbers (nCount), mapping rates and tdTomato reads numbers (nCounts tdTm) for all chimeric cells (left four panels). The gene expression levels and tSNE plot of control monkey (Control-Monkey) and host monkey (Chimera-Monkey) cells before and after integration (remove batch effect) (right two panel).

(D) The bubble charts showing the expression of the reported marker genes in chimeric human EPI-like (Chimera Human EPI), HYP-like (Chimera Human HYP), and TE-like (Chimera Human TE) cells, respectively.

(E) Heatmap showing the expression of lineage markers conserved between humans and monkeys in chimeric human EPI-like, HYP-like, and TE-like cells. EPI, epiblast; HYP, hypoblast; TE, trophectoderm.

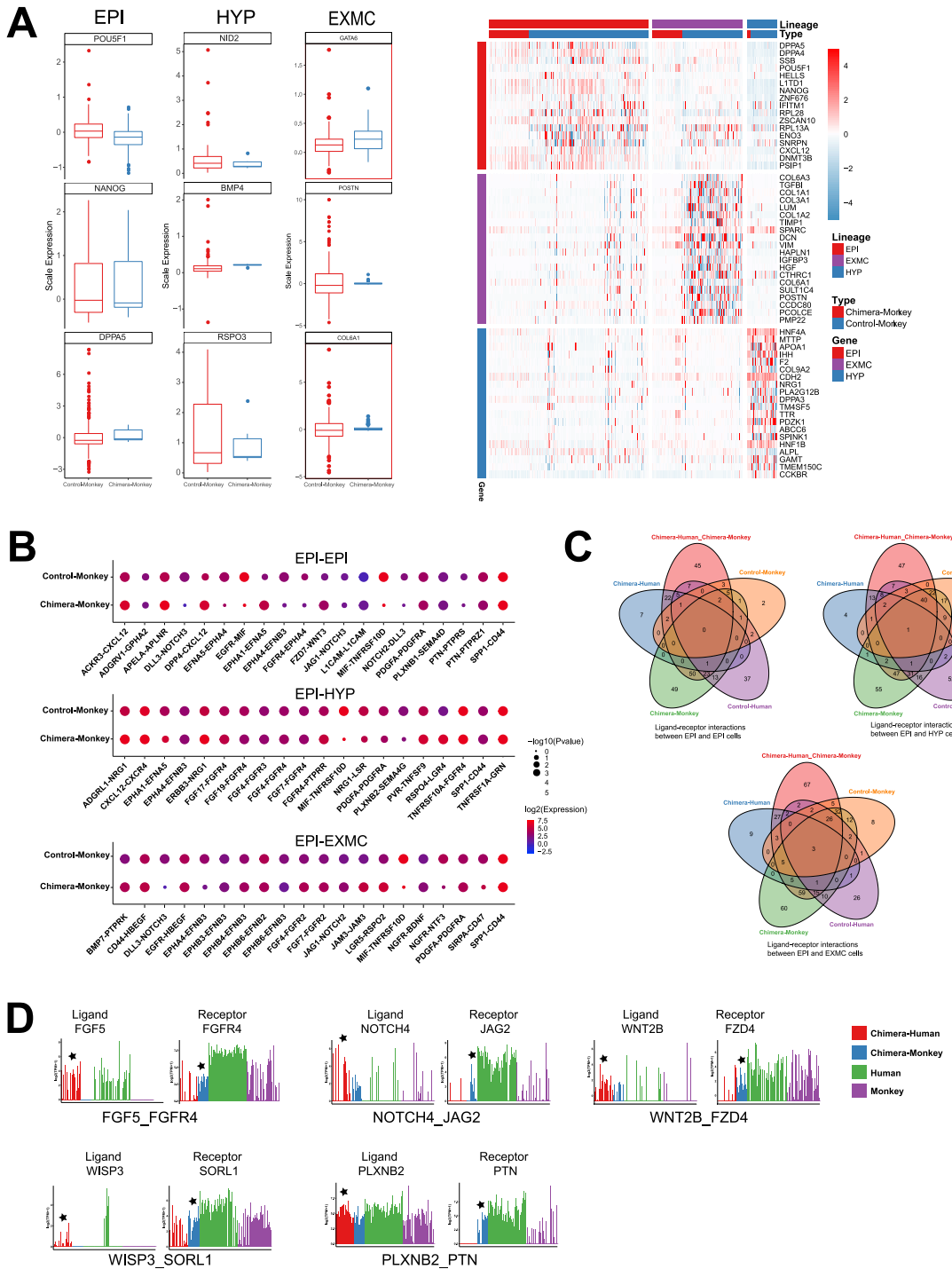

Figure S3. Comparative analysis of monkey cells between the chimeric and host embryos, related to Figure 4

(A) Boxplot (left panels) and heatmap (right panel) showing expression of marker genes for EPI, HYP, and EXMC lineages between the chimeric (Chimera-Monkey) and control (Control-Monkey) embryos.

(B) The top 20 ligand-receptor interactions between EPI-EPI, EPI-HYP and EPI-EXMC, respectively, non-chimeric monkey (Control-Monkey) cells are used as control to compare with chimeric cells (Chimera-Monkey).

(C) Venn diagram showing the common and specific ligand-receptor interactions between EPItoEPI, EPItoHYP, and EPItoEXMC in distinct cells.

(D) The expression levels (log2 [TPM+1]) of the representative ligand-receptors interactions between chimeric human (Chimera-Human) and host monkey (Chimera-Monkey) EPI cells are shown. EPI, epiblast; HYP, hypoblast; EXMC, extra-embryonic mesenchyme cell. Human, control human EPI cells (Zhou et al., 2019); Monkey, control monkey EPI cells (Niu et al., 2019).

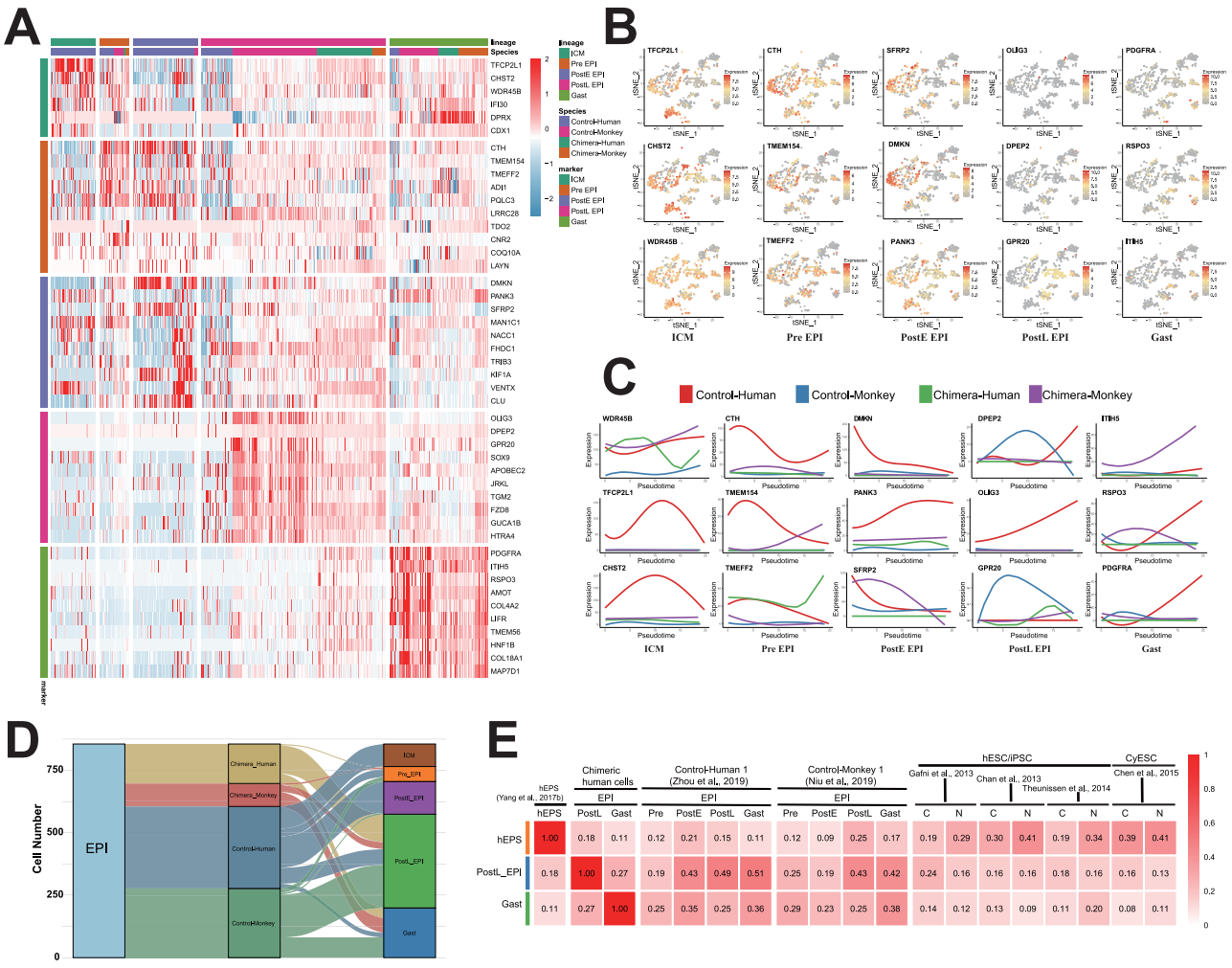

Figure S4. Characteristics of subgroups in the EPI lineage, related to Figure 5

(A) Heatmap of the expression levels of identified marker genes for the subgroups of ICM, Pre_EPI, PostE_EPI, PostL_EPI, and Gast.

(B) Expression of subgroup-specific marker genes exhibited on t-SNE plots. A gradient of gray, yellow, and red indicates low to high expression.

(C) The dynamic change of marker genes for different subgroups along the pseudotime.

(D) The sankey diagram showing the number and flow from different cell types to different lineages.

(E) Heatmap of the correlation coefficients among hEPSCs (Yang et al., 2017b), chimeric human EPI-like (Chimeric human) cells, and control human (Control-Human 1) and monkey (Control-Monkey 1) EPI cells (Niu et al., 2019; Zhou et al., 2019) and human (hESC/iPSC) and monkey (CyESC) PSCs at primed (C) or naive (N) pluriotency state (Chan et al., 2013; Chen et al., 2015; Gafni et al., 2013; Theunissen et al., 2014). ICM, inner cell mass; EPI, epiblast; Pre_EPI, pre-implantation EPI; PostE_EPI, post-implantation early EPI; PostL_EPI, post-implantation late EPI; Gast, gastrulating cell; N, 'naive'; C, conventional (primed).

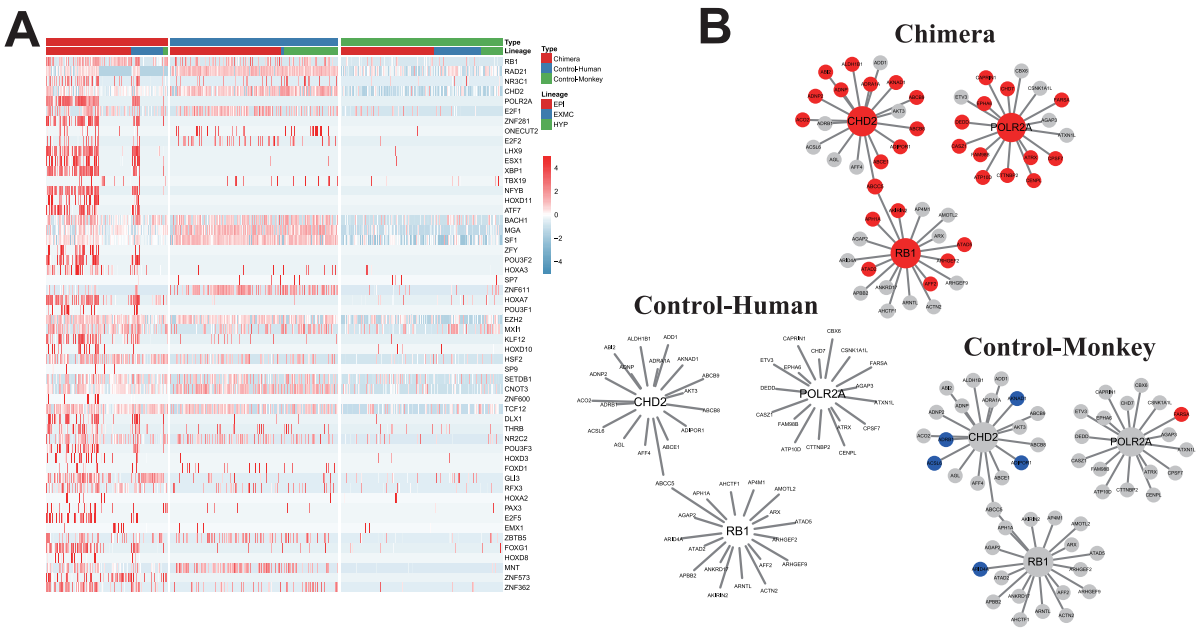

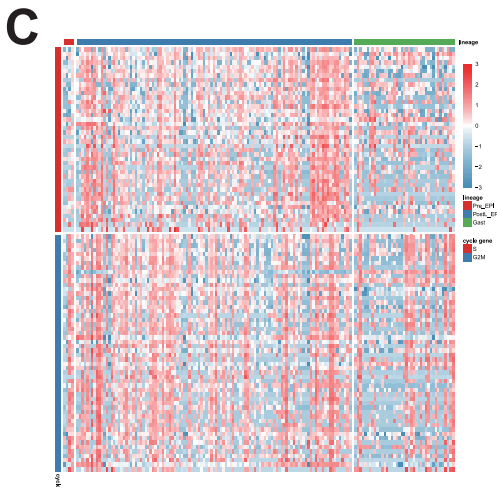

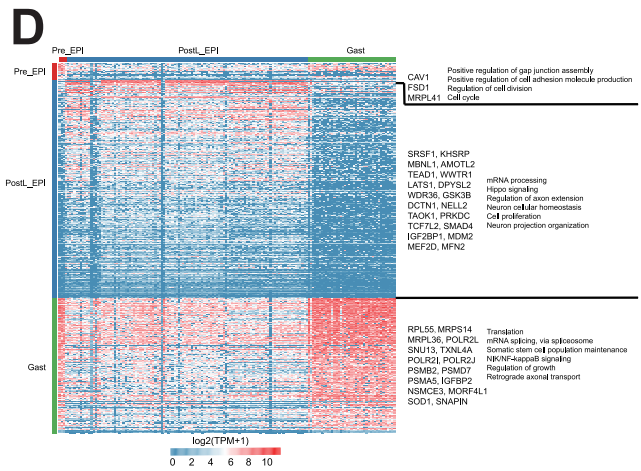

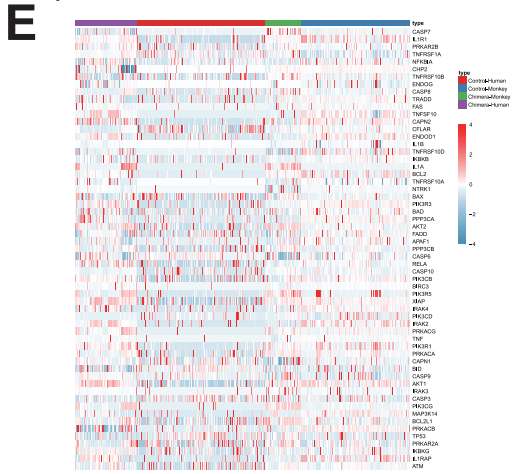

(legend on next page)

Figure S5. Regulatory network analysis of chimeric EPI cells, related to Figure 5

(A) The regulon-activity heatmap for the chimeric (Chimera) EPI cells with human and monkey non-chimeric (Control-Human and Control-Monkey) embryos as controls. The samples in each column were ordered based on lineage and species origins. These regulons are specific for chimeric EPI cells. (B) Regulatory networks of the top 3 regulons for non-chimeric control human (Control-Human), monkey (Control-Monkey) and chimeric (Chimera) EPI cells. The gene expression status (up, down, and no change) are colored with red, blue, and gray, respectively. The transcription factors located in the center regulate the surrounding target genes. (C) Heatmap showing the expression levels of cell-cycle related genes in chimeric human EPI-like cells. Cell-cycle related genes were retrieved from Seurat package (v.3.1.1). (D) Heatmap showing the expression levels of the markers identified from EPI sub-groups and the related biological processes. (E) Heatmap showing the expression of apoptosis related genes in control human (Control-Human), control monkey (Control-Monkey), host monkey (Chimera-Monkey) and chimeric human (Chimera-Human) cells. Apoptosis related genes were obtained from GSEA website. Pre_EPI, pre-implantation EPI; PostL_EPI, post-implantation late EPI; Gast, gastrulating cell